Bidirectional control of orienting behavior by distinct prefrontal circuits

Rafiq Huda[1], Grayson O. Sipe[1], Elie Adam[1], Vincent Breton-Provencher[1], Gerald Pho[1], Liadan Gunter[1], Ian R. Wickersham[2] & Mriganka Sur[1*]

[1]Picower Institute for Learning and Memory
Department of Brain and Cognitive Sciences
Massachusetts Institute of Technology, Cambridge, MA 02139, USA
[2]McGovern Institute for Brain Research
Massachusetts Institute of Technology, Cambridge, MA 02139, USA

*Corresponding author (msur@mit.edu)

Abstract

The prefrontal cortex (PFC) orchestrates voluntary behavior by biasing activity in downstream structures to promote actions consistent with current task goals while inhibiting inconsistent ones. PFC circuits comprise of vastly converging inputs and diverging outputs, but how this anatomical diversity allows it to bidirectionally control specific behaviors remains unclear. Here we use multiple approaches to show that a subdivision of the mouse PFC, the anterior cingulate cortex (ACC), integrates and routes discrete sensory inputs to anatomically segregated populations of projection neurons in order to promote and inhibit goal-directed visual orienting responses. Surprisingly, ACC outputs to the superior colliculus principally inhibit incorrect orienting movements. Optogenetic analyses and a projection-based activity model make the unexpected prediction that feedback from the ACC to the visual cortex is critical for correct orienting, which we confirm. Integrating anatomically non-overlapping but functionally complementary projections for bidirectional control may be a general organizing principle for PFC circuits.

Animals respond to their environments using complex and diverse motor movements, but are limited by being able to enact only single actions at a time. Hence, voluntary control over behavior requires context-dependent mechanisms that select appropriate actions and suppress complementary but inappropriate ones. Such duality of behavioral control is readily apparent in sets of commonly displayed opposing behaviors, such as freeze/flight, approach/avoidance, and exploration/exploitation[1–6]. The prefrontal cortex (PFC) has been widely implicated in dynamically coordinating behavior by biasing the flow of activity in downstream cortical and subcortical structures[7–11], but a fundamental outstanding question is how the anatomical organization of inputs to and outputs from the PFC enables its proposed role. An emerging theme from recent studies is that the PFC uses distinct output circuits to promote and suppress innate behaviors such as conditioned fear responses[12,13], reward-seeking[14–16], and social interactions[17]. The behavioral repertoire of animals is highly enriched by their ability to learn arbitrary associations between environmental sensory cues and motor movements[18–21]. Bilateral orienting (such as turn left or right) to sensory cues is a fundamental action at the core of a wide range of such learned sensorimotor behaviors[22–27] and involves mechanisms that select and suppress specific orienting movements[28]. Unlike other dual behaviors that often consist of asymmetric action-inaction pairs[14,17,29], orienting involves a symmetrical pair of actions (expression of each action has a counter action that was suppressed), making it an attractive model for studying bidirectional control of behavior. Orienting behavior also requires activity in the PFC[30–34], but the circuit-level mechanisms by which the PFC generates signals for bilateral control are unclear. Here, we use a combination of virus-mediated anatomical tracing, two-photon imaging of inputs/outputs, and projection-specific optogenetics to show that a subdivision of the mouse PFC, the anterior cingulate cortex (ACC), uses distinct projection neuron populations to promote and suppress goal-directed orienting.

Cortico-cortical and cortico-collicular circuits for bilateral visual orienting

Bilateral visually-guided orienting crucially requires integration of inputs from the two halves of the visual field. Recent anatomical and functional studies in mice suggest a role for the ACC in coordinating visual behavior[30,31,35,36]. However, it is unclear if the ACC contains a subregion anatomically specialized for the control of bilateral orienting.

Injection of rabies viruses encoding GFP and tdTomato into caudal and rostral ACC (Fig. 1A) showed that although both compartments received inputs from medial higher visual cortex, corresponding to functionally-defined anteromedial and posteromedial areas[37], the caudal ACC also received inputs from the primary visual cortex (Fig. 1B-C). Each compartment also received prominent inputs from the contralateral hemisphere spanning the entire extent of the ACC (Fig. 1D), suggesting that visual information relayed from the visual cortex (VC) may be exchanged between ACC hemispheres via callosal projections. We tested this possibility by using two-photon microscopy to image visually-evoked GCaMP6s responses of VC and callosal axons in the ACC (Fig. 1E). While VC axons responded nearly exclusively to stimuli presented in the contralateral visual field (relative to the site of recording), callosal axons responded preferentially to ipsilateral stimuli (Figs. 1F, G; Extended Data Figs. 1, 2). In addition, we found that the caudal ACC sends outputs to the ipsilateral motor-related layers of the superior colliculus (SC_m; Fig. 1H-J), a midbrain structure that coordinates visually-driven contraversive orienting movements[38]. These anatomical and functional observations, together with previous studies demonstrating that visual cortical areas have largely lateralized representations of stimuli and callosal connectivity limited to the midline of the visual field[37,39], suggest that the caudal ACC is uniquely positioned to integrate extended visual inputs presented in either hemifield and may bidirectionally control behavioral responses to them by influencing activity in SC_m (Fig. 1K).

To test this possibility, we designed a task for head-fixed mice, modified from a previous design[27], that allowed us to dissect the role of ACC in promoting and inhibiting visual orienting behavior. Head-fixed mice are unable to orient with head or whole-body movements; hence, we trained mice to orient to visual cues with their forepaws. We trained mice to simultaneously learn two forepaw orienting movements so that no particular action is reflexive and the selection of each requires simultaneous suppression of the other. Mice had to orient to the spatial location of a visual cue presented in either hemifield by rotating a trackball along a fixed axis with their forepaws to the left or right (Fig. 2A, B). We provided visual feedback by coupling the rotation of the trackball to the location of the stimulus on the screen in closed-loop such that correct performance required mice to move the presented visual cue to the center of the screen. Importantly,

the use of lateralized visual cues allowed us to make precise predictions about the flow of sensory information along anatomical pathways revealed by our tracing experiments (Fig. 1K). Trials in which mice rotated the trackball in the direction opposite to that instructed by the cue were considered incorrect and allowed a dissociation of neural signals that process sensory or movement information. We used a reaction time task-design that allowed mice to move as soon as they could after stimulus onset. This minimized potential confounds of short-term memory and extensive movement planning associated with delay tasks[40]. We first tested trained mice with stimuli of varying luminance and found that behavioral performance was dependent on stimulus strength (Extended Data Fig. 3A). We increased task difficulty by simultaneously presenting two visual cues with different luminance intensities and requiring mice to select the cue with the higher luminance. We found that performance was perceptually limited by the difference in luminance of the two stimuli (Extended Data Fig. 3B). Hence, we reduced perceptual ambiguity by presenting single, high luminance visual cues. Under these conditions, performance errors are unlikely to be due to perceptual errors and likely reflect the failure to execute the correct or suppress the incorrect movement. Experienced mice performed well on this task (~90% accuracy), moving the ball rapidly at short latencies (~200ms) after stimulus onset (Extended Data Fig. 3C-G).

Next, we conceptualized a circuit diagram for an orienting system in which the ACC promotes and inhibits behavior by sending bias signals that directly or indirectly modulate activity in SC_m (Fig. 2C). We reasoned that VC and callosal inputs allow ACC neurons in each hemisphere to represent both contralateral and ipsilateral stimuli and coordinate orienting responses to them. In our task, an ipsiversive orienting movement requires concurrent suppression of the contraversive movement; hence, ACC neurons active on ipsiversive orienting trials may recruit pathways that suppress activity in SC_m to inhibit erroneous contraversive orienting. Similarly, other ACC neurons may recruit pathways that enhance activity in SC_m to promote correct contraversive orienting.

VC provides sensory inputs to, and SC_m provides motor outputs of, the orienting system

We used optogenetics to first determine the contribution of the input and output structures of the orienting system, the VC and SC_m, to task performance. Illuminating the cortex or

118 SC_m with blue or orange light in the absence of an opsin did not produce significant
119 changes in behavior (Extended Data Fig. 4). In contrast, unilaterally inactivating the VC
120 by delivering orange light onto Jaws-expressing neurons increased the error rate on
121 contraversive trials and decreased contraversive orienting (Fig. 2D, G). While this
122 manipulation did not change the movement start time or velocity, there was an increase
123 in the miss rate (i.e., trials in which no response is made) on contralateral stimulus trials
124 (Extended Data Fig. 5A). The VC projects to various brain areas in addition to the ACC.
125 Hence, we used projection-specific optogenetics to evaluate the necessity of direct VC
126 inputs to the ACC in our task. Photoinhibition of Jaws-expressing VC axons in the ACC
127 increased contraversive errors without affecting performance on ipsilateral stimulus trials
128 (Fig. 2E, G). Moreover, it decreased the movement velocity on correctly performed
129 contraversive trials, but there was no change in the miss rate or the movement start time
130 for either trial-type (Extended Data Fig. 5B). These results demonstrate that the VC is
131 necessary for the detection of visual stimuli and that its inputs to the ACC promote
132 contraversive movements by biasing activity in the orienting system.

133 Unilateral inactivation of SC_m by illuminating Jaws-expressing neurons with orange
134 light dramatically reduced contraversive orienting (Fig. 2F, G), similar to that shown for
135 naturalistic orienting behaviors[38,41], and consistent with our hypothesis that SC_m is an
136 output node of the orienting system (Fig. 2C). Photoinhibition of SC_m did not grossly inhibit
137 motor function, as there was no change in the miss rate, the movement start time or
138 velocity (Extended Data Fig. 5C). Interestingly, inhibiting activity unilaterally in SC_m had
139 a bidirectional effect on orienting behavior: although it reduced performance on
140 contraversive trials, it also improved performance on ipsiversive trials (Fig. 2F). Such
141 stimulus-dependent, opposing effects of SC activity on orienting behavior may be
142 mediated via interhemispheric mutual inhibition between the two sides of the SC[26,41] or
143 may rely on extrinsic inputs that selectively control orienting responses to contralateral
144 and ipsilateral stimuli by increasing or decreasing activity in SC_m.

145 Having established the inputs to and outputs of the orienting circuit, we asked how
146 its key node, the ACC, conveys critical signals for the task. Our observation that the ACC
147 receives information about both contralateral and ipsilateral stimuli (Figs. 1A-G; Extended
148 Data Figs. 1, 2) suggests that it integrates this information to differentially modulate

activity in SC_m through distinct output pathways. Hence, we used projection-specific recordings and activity manipulations to critically evaluate the contribution of discrete ACC output pathways to SC_m.

Activity of ACC-SC neurons predicts ipsiversive orienting

We first evaluated the role of direct ACC outputs to SC_m to orienting in our task. We measured the calcium responses of GCaMP6s-expressing layer 5 neurons during the task and identified back-labeled ACC-SC neurons by injecting a retrograde tracer into SC_m (Fig. 3A). Examination of single neuron responses on correct trials, with data aligned to stimulus onset, showed robust task-related activity in ACC-SC (Fig. 3B) and unlabeled neuron populations (Extended Data Fig. 7A). While some individual neurons were active during contraversive or ipsiversive orienting trials, others responded during either trial-type. We identified task-modulated neurons by comparing activity before and after stimulus onset. A majority of ACC-SC neurons imaged during the task (60.1%) showed task-modulated activity. Next, we computed a trial preference score for each task-modulated neuron and used a permutation test ($p < 0.05$) to find cells that were preferentially active on contraversive or ipsiversive trials (Fig. 3C, D; Extended Data Fig. 6B). Overall, 65% of ACC-SC neurons with significant trial preference were active on correct contraversive and 35% on correct ipsiversive trials, suggesting that the ACC-SC pathway coordinates bilateral orienting. Since we observed a similar pattern of activity between ACC-SC and unlabeled neurons, it is likely that additional ACC output pathways also contribute to orienting behavior in our task.

Next, we investigated whether task-responses of ACC-SC neurons represent the location of the stimulus or the direction of the orienting movement. We reasoned that since the same visual cue is presented on either correct or error trials, neurons representing the stimulus would respond similarly under both conditions. Likewise, since animals make opposite orienting movements on these trials, we would expect neurons that represent the movement direction to have different activity. We differentiated between responses on contraversive and ipsiversive trials by comparing the activity of ACC-SC neurons preferentially active on either trial-type. Examining single-neuron and population averaged responses showed that contra-preferring ACC-SC neurons responded largely similarly on correct and error trials (Extended Data Fig. 7A-C). In

contrast, responses of ipsi-preferring ACC-SC neurons were differentially modulated (Extended Data Fig. 7D-F). We further examined this phenomenon by training linear decoders with single-trial responses of contra- or ipsi-preferring ACC-SC neurons to predict the location of the visual cue (cue decoder) or the direction of the orienting movement (movement decoder; Fig. 3E; see Methods). Decoders trained with the activity of either contra- or ipsi-preferring ACC-SC neurons performed better than chance at predicting the visual cue location or the movement direction (compared to shuffled data, $p < 0.01$). However, cue decoders trained with the activity of contra-preferring ACC-SC neurons were better at predicting the location of the visual cue, whereas movement decoders trained with the activity of ipsi-preferring neurons were better at predicting the movement direction (Fig. 3F). Thus, while contra-preferring ACC-SC neurons contain more cue information, ipsi-preferring ACC-SC neurons contain more movement information.

ACC-SC pathway inhibits incorrect contraversive orienting

ACC-SC neurons are active on contraversive and ipsiversive trials (Fig. 3C), suggesting that they modulate both orienting movements. We tested this by expressing Jaws or eNpHR3.0 in excitatory ACC neurons and locally inactivating ACC outputs to SC_m during the task (Fig. 4A, B). In surprising contrast to our original hypothesis (Fig. 2C), inactivating the ACC-SC output pathway decreased performance on ipsiversive trials but had no effect on contraversive trials (Fig. 4C). Thus, the ACC-SC pathway is principally engaged during ipsiversive trials to suppress erroneous contraversive orienting. We previously showed that activity in SC_m promotes contraversive orienting (Fig. 2F, G). Hence, this result suggests that the ACC-SC pathway specifically inhibits the SC_m to suppress incorrect orienting (Fig. 4D).

Projection optogenetics non-specifically inhibits ACC outputs to SC_m, making it difficult to isolate the contribution of ipsiversive responses of ACC-SC neurons to activity in SC_m. We reasoned that since callosal axons convey sensory information for ipsiversive orienting (Fig. 1F, G; Extended Data Fig. 2), photoactivating them would recruit ACC-SC neurons that suppress activity in SC_m. We unilaterally expressed ChR2 in excitatory ACC neurons and placed an optic fiber cannula in the opposite ACC to target callosal inputs. We made extracellular recordings of spontaneous activity with a 16-channel silicone

probe in the SC_m ipsilateral to the site of the implanted fiber and activated callosal inputs with blue light (Fig. 4E, F). Laser activation of callosal ACC axons modulated the activity of 32.4% (24/75) of isolated single SC_m units (Wilcoxon signed-rank test, $p < 0.05$). Inspection of single-neuron responses showed a time-locked decrease in activity with laser activation (Fig. 4G). Quantifying the effect of callosal photostimulation on the activity of all laser-modulated SC_m neurons showed that this manipulation led to a significant net decrease in activity (Fig. 4H). As a comparison, directly activating ChR2-expressing ACC neurons (Extended Data Fig. 8A, B) modulated the activity of a similar proportion of units in the ipsilateral SC_m as in the previous experiment (27.0%, 17/63 units from 3 mice), but individual neurons had both increased and decreased activity (Extended Data Fig. 8C, D). As a result, there was no net change in the activity of the population of laser-modulated neurons (Extended Data Fig. 8E). Hence, while selectively activating callosal ACC inputs inhibits SC_m, direct activation has a more heterogeneous effect, suggesting that callosal inputs carrying ipsilateral stimulus information to the ACC recruit ACC-SC neurons to specifically suppress SC_m activity.

Long-range cortical outputs are primarily glutamatergic and it is unclear how callosal activation suppresses activity in SC_m. We used anterograde transsynaptic viral tracing to test the possibility that ACC outputs target inhibitory neurons in SC_m[42]. We injected tdTomato reporter mice with an AAV1 virus expressing the Flpo recombinase in the ACC (Extended Data Fig. 9A) and performed immunohistochemistry against GABA in slices containing the SC_m (Extended Data Fig. 9B, C). Counting cells positive for tdTomato and GABA showed that ~30% of SC_m neurons that receive inputs from the ACC contained GABA and hence are likely to be inhibitory neurons (Extended Data Fig. 9D). Therefore, recruiting local inhibition in SC_m is a possible mechanism by which ACC-SC neurons inhibit activity in SC_m. to suppress erroneous contraversive orienting (Fig. 4D).

ACC-VC pathway promotes correct contraversive orienting

Although the ACC-SC pathway is primarily engaged during ipsiversive orienting, calcium imaging of non-SC projecting ACC neurons revealed robust responses on contraversive trials (Extended Data Fig. 6B), suggesting that the ACC also contributes to correct contraversive orienting. We tested this by photostimulating ChR2-expressing inhibitory neurons in the ACC with blue light to inactivate it during the task. ACC inactivation

242 produced similar changes in behavior as observed with inactivation of SC_m (Fig. 2F, G)
243 and led to an overall decrease in contraversive orienting (Fig. 5A). Furthermore, this
244 manipulation did not change the miss rate or movement start time, but reduced movement
245 velocity on contraversive orienting trials (Extended Data Fig. 10). Thus, activity in ACC is
246 necessary for correct contraversive orienting.

247 This finding is surprising because if ACC-SC neurons suppress the SC_m during
248 ipsiversive orienting, inactivating the ACC should disinhibit SC_m activity on these trials
249 and increase contraversive orienting. Hence, regional inactivation of the ACC, which
250 simultaneously manipulates activity across a range of output pathways that provide
251 extrinsic inputs to SC_m[43], must exert its effect through another ACC output that promotes
252 contraversive orienting. Regional inactivation of the VC showed that it promotes
253 contraversive orienting (Fig. 2D). Moreover, the ACC sends dense outputs to the
254 VC[35,43,44] and controls the gain of its sensory responses[35]. The VC in turn projects to and
255 modulates activity in the SC[45], suggesting that the ACC-VC pathway may drive
256 contraversive orienting by indirectly modulating activity in the SC_m (Fig. 5B). We set up a
257 linear model based on the anatomical, functional, and behavioral data obtained thus far
258 to better understand how projections between ACC, VC, and SC_m interact to produce the
259 observed behavioral performance (Extended Data Fig. 11A; see complete details in
260 Methods). We were specifically interested in formally testing our reasoning that the ACC-
261 VC pathway indirectly excites the SC and promotes contraversive orienting, thus
262 reconciling the conflicting results obtained with regional ACC and ACC-SC inactivation
263 experiments. We defined the activity of each SC_m hemisphere as a linear sum of four
264 input pathways on contraversive and ipsiversive trials: 1) direct ACC-SC pathway that
265 excites the SC on contra trials, 2) direct ACC-SC pathway that inhibits the SC on ipsi
266 trials, 3) an ACC-VC pathway that indirectly excites the SC on contra trials (ACC-VC-SC),
267 and 4) a pathway representing the baseline task-independent activity of the SC. Based
268 on previous studies[26], we modeled behavioral performance as a function of the difference
269 in activity between the two hemispheres of SC_m such that the side with higher activity
270 leads to its preferred contraversive orienting movement (Extended Data Fig. 11B). We
271 represented three crucial optogenetic experiments (inactivation of ACC, SC, and ACC
272 projections to the SC; Extended Data Fig. 11C) in the model and used the behavioral

performance observed on them to derive estimates for the contribution of these four pathways to activity in SC_m during the task (Extended Data Fig. 11D, E). Next, we simulated the inactivation of ACC outputs to the VC in the model (Extended Data Fig. 11D); using these estimates led to the prediction that the ACC-VC-SC pathway promotes contraversive orienting (Extended Data Fig. 11E). Hence, inactivating ACC outputs to the VC should decrease contraversive orienting.

Since our model predicted that the ACC-VC and ACC-SC pathways make opposing contributions to orienting, we first tested if there is anatomical segregation in the population of ACC neurons that project to these areas. We injected rabies viruses encoding either GFP or tdTomato in the VC and SC_m and quantified the number of backlabeled neurons in the ACC. Consistent with a previous study[43], we found that non-overlapping sets of ACC neurons targeted these structures (Fig. 5C-D). Next, we directly tested the model prediction that the ACC-VC pathway drives contraversive orienting by expressing Jaws in the ACC and placing a chronic window over the VC to inactivate ACC output axons during the task (Fig. 5E). Inactivating the ACC-VC pathway decreased contraversive orienting (Fig. 5F, G), as predicted by the model (Extended Data Fig. 11). Comparing the effect of inactivating the ACC-SC and ACC-VC pathways showed that ACC outputs to SC_m suppress, and outputs to VC promote, contraversive orienting (Fig. 5G). Together, our results show that the ACC uses distinct population of projection neurons, driven by distinct visual stimuli, to either promote or inhibit orienting behavior (Fig. 5B).

Discussion

Our experiments identify specific inputs to and outputs from PFC that together coordinate bidirectional control of orienting behavior. We show that VC inputs bring information about the contralateral stimulus whereas callosal inputs convey the presence of ipsilateral stimuli to the ACC (Fig. 1A-G; Extended Data Figs. 1, 2). Using an SC_m-dependent forepaw orienting task in head-fixed mice that also requires activity in the VC and the ACC (Fig. 2D-G), we show that these inputs enable the modulatory role of ACC, as calcium imaging of task-responses from ACC neurons show that individual neurons are preferentially active on both contraversive and ipsiversive trials (Fig. 3C; Extended Data Fig. 6B). The activity of ACC-SC neurons predicts ipsiversive movements (Fig. 3F).

304 Mimicking the presence of cues instructing ipsiversive orienting through photostimulation
305 of callosal inputs potentially recruits local inhibition to suppress activity in SC_m (Fig. 4E-
306 H). Furthermore, disinhibiting SC_m by removing this inhibitory drive increases erroneous
307 contraversive orienting on ipsiversive trials (Fig. 4A-D). At the same time, inactivation of
308 a parallel output pathway from the ACC to the VC inhibits correct orienting on
309 contraversive trials (Fig. 5F). Thus, the ACC-SC pathway inhibits incorrect contraversive
310 orienting, whereas the ACC-VC pathway promotes correct contraversive orienting (Fig.
311 5B, G).

312 Each hemisphere of SC_m coordinates contraversive orienting movements (Fig. 2F,
313 G) and competition between the two sides of SC_m via mutual inhibition has been proposed
314 as a potential mechanism underlying performance in two-choice orienting tasks[26]. Our
315 results suggest that such a competition first takes place within each hemisphere of SC_m
316 and is arbitrated through distinct PFC output pathways that increase or decrease activity
317 levels in the SC_m to promote or suppress specific orienting movements. Due to the
318 lateralized nature of stimulus representation in the visual system, the ACC likely
319 constitutes one of very few extrinsic inputs to SC_m that represent the ipsilateral stimulus
320 and hence can serve uniquely to suppress erroneous contraversive movements in the
321 presence of such stimuli. In agreement, we found that although direct photostimulation of
322 the ACC had a heterogeneous effect on the activity of SC_m, selective activation of callosal
323 inputs, which represent ipsilateral stimuli (Fig. 1F, G; Extended Data Fig. 2), suppressed
324 activity in SC_m (Fig. 4G, H). Although the simplest interpretation of these results is that
325 callosal activation recruits a subset of ACC-SC neurons that directly inhibit SC_m by
326 recruiting local inhibition (Extended Data Fig. 9), we cannot rule out the possibility that
327 these inputs recruit ACC projections to an intermediary area(s) which then inhibits SC_m.
328 Nonetheless, using projection-specific optogenetics during the task, we provide clear
329 evidence that direct projections from ACC to SC_m exert inhibitory control over behavior
330 by suppressing incorrect contraversive orienting (Fig. 4C, D).

331 While responses of ACC-SC neurons on ipsiversive trials are necessary for this
332 inhibitory control, our experiments show that ACC-SC neurons are also active on
333 contraversive trials (Fig. 3C). However, ACC inputs to SC_m are not necessary for
334 contraversive orienting under our task conditions (Fig. 4C). This suggests that the

335 contribution of ACC inputs to contraversive orienting may be redundant to inputs that the
336 SC_m receives from other sources. Our decoding analysis suggests that these neurons
337 predominantly carry stimulus information (Fig. 3F). The sensory layer of the SC receives
338 strong visual drive directly from the retina and the visual cortex[39,46], and can drive
339 orienting movements via feedforward projections to SC_m[47]. Thus, inputs from the sensory
340 SC may compensate for ACC inputs on contraversive trials to SC_m.

341 Although ACC inputs to SC_m inhibit contraversive orienting, we found that the ACC
342 uses an anatomically non-overlapping but functionally complementary population of
343 projection neurons to promote orienting behavior through the visual cortex (Fig. 5F, G).
344 Remarkably, both VC inputs to ACC (Fig. 2E), and outputs back from ACC to VC, are
345 crucial for contraversive orienting. These results are consistent with a recent study
346 showing that photoactivation of ACC outputs to the VC promotes contraversive turning in
347 locomoting mice traversing a virtual corridor[44] and with studies in monkeys showing that
348 stimulation of the visual cortex evokes saccadic eye movements[48]. While the exact
349 mechanisms mediating orienting responses through the visual cortex are unclear, ACC
350 outputs to VC may promote contraversive orienting behavior by controlling VC outputs to
351 multiple pathways that converge in SC_m[45,49,50].

352 Similar to previous studies[20,22], we also found that non-discriminate, regional
353 inactivation of an area in the frontal cortex decreased contraversive orienting (Fig. 5A),
354 which at first sight would suggest that it only promotes such behavior. However, our
355 results highlight the difficulty in ascribing functional roles to specific brain areas by using
356 only regional inactivation. Such manipulations simultaneously change activity across
357 multiple output pathways and thus obscure the effect of individual, potentially
358 antagonistic, outputs. By dissecting the contribution of individual outputs, our results
359 highlight a candidate long-range circuit motif for PFC circuits wherein anatomically non-
360 overlapping but functionally complementary output projections exert control over common
361 downstream motor structures to promote and inhibit orienting behavior.

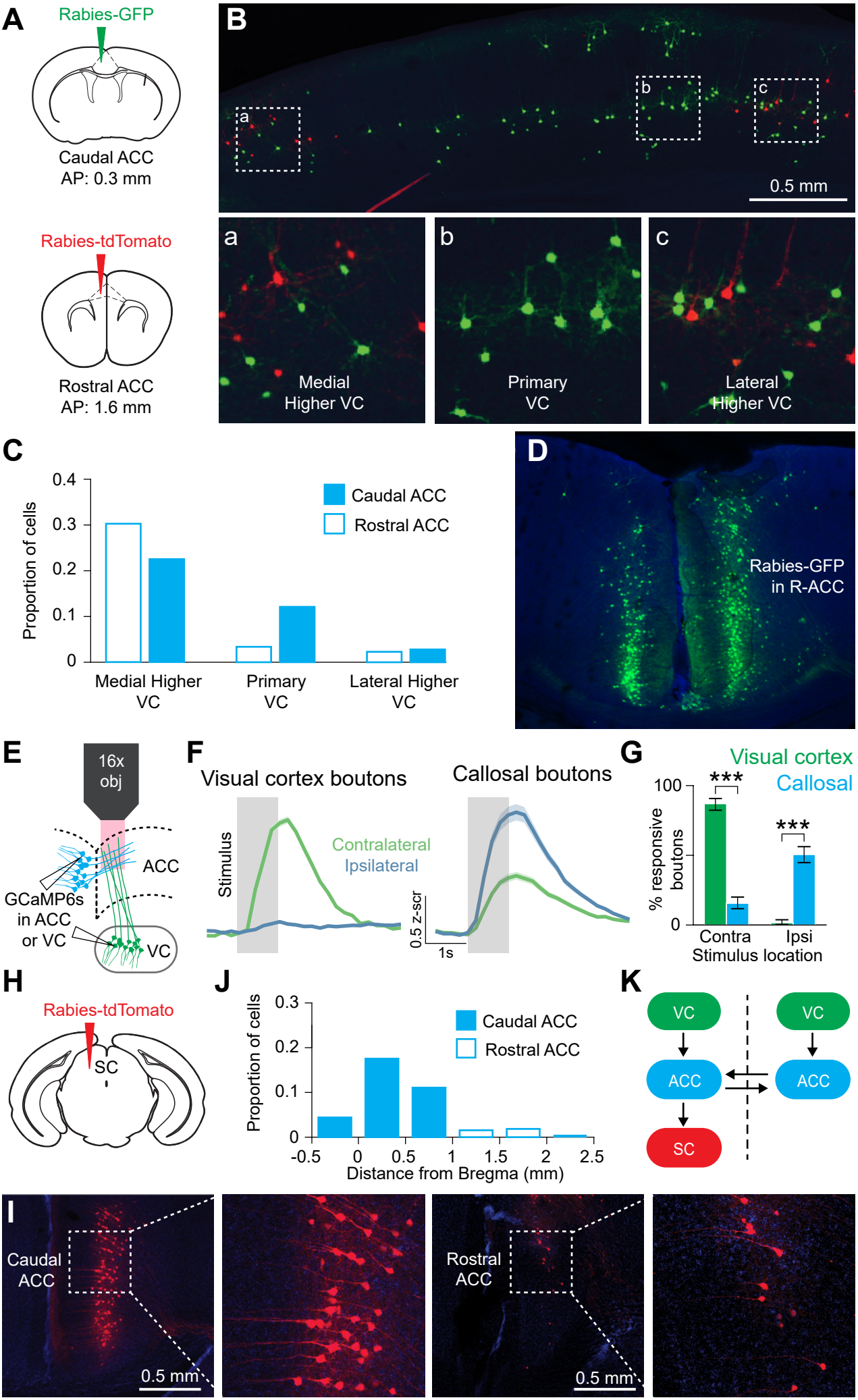
A
Rabies-GFP
Caudal ACC
AP: 0.3 mm
Rabies-tdTomato
Rostral ACC
AP: 1.6 mm
B
a
b
c
0.5 mm
Medial
Higher VC
Primary
VC
Lateral
Higher VC
C
Proportion of cells
0.4
0.3
0.2
0.1
0
Caudal ACC
Rostral ACC
Medial Higher VC
Primary VC
Lateral Higher VC
D
Rabies-GFP
in R-ACC
E
16x
obj
ACC
GCaMP6s
in ACC
or VC
VC
F
Visual cortex boutons
Callosal boutons
Stimulus
Contralateral
Ipsilateral
0.5 z-scr
1s
G
Visual cortex
Callosal
100
0
***
***
% responsive
boutons
Contra
Ipsi
Stimulus location
H
Rabies-tdTomato
SC
J
Proportion of cells
0.3
0.2
0.1
0
Caudal ACC
Rostral ACC
-0.5
0
0.5
1
1.5
2
2.5
Distance from Bregma (mm)
K
VC
VC
ACC
ACC
SC
I
Caudal
ACC
0.5 mm
Rostral
ACC
0.5 mm

Figure 1

Figure 1. Anatomical and functional characterization of inputs to and outputs from the ACC. A) Rabies viruses encoding GFP or tdTomato were injected into caudal or rostral ACC, respectively. B) Back-labeled neurons in the visual cortex. Neurons in medial higher VC, primary VC, or lateral higher VC are denoted by dotted squares (a-c) on top and shown at higher magnification on the bottom. C) Proportion of back-labeled neurons in various VC subdivisions projecting to caudal (solid) or rostral (unfilled) ACC (n = 3 animals). D) Back-labeled callosal caudal ACC neurons. E) Experimental setup for two-photon imaging of GCaMP6s-expressing visual cortex or callosal axons in the ACC while head-fixed mice passively viewed visual stimuli (black square or grating, ~20º) presented in either hemifield. F) Population-averaged responses of visually-driven VC (n = 268 boutons from 5 mice) and callosal (n = 309 boutons from 4 mice) boutons to stimuli presented in contra- and ipsilateral hemifield. G) Percent of visually-driven VC and callosal boutons with preferential responses to contra or ipsi stimuli. Errors bars are 95% binomial confidence intervals. ***$p < 0.005$ (Fisher's exact test). H) Rabies virus encoding tdTomato was injected in the SC. I) Back-labeled caudal and rostral ACC neurons projecting to the SC. J) Proportion of SC back-labeled neurons along the anterior-posterior axis of the ACC (n = 2 animals). K) Schematic of inputs to and outputs from the caudal ACC.

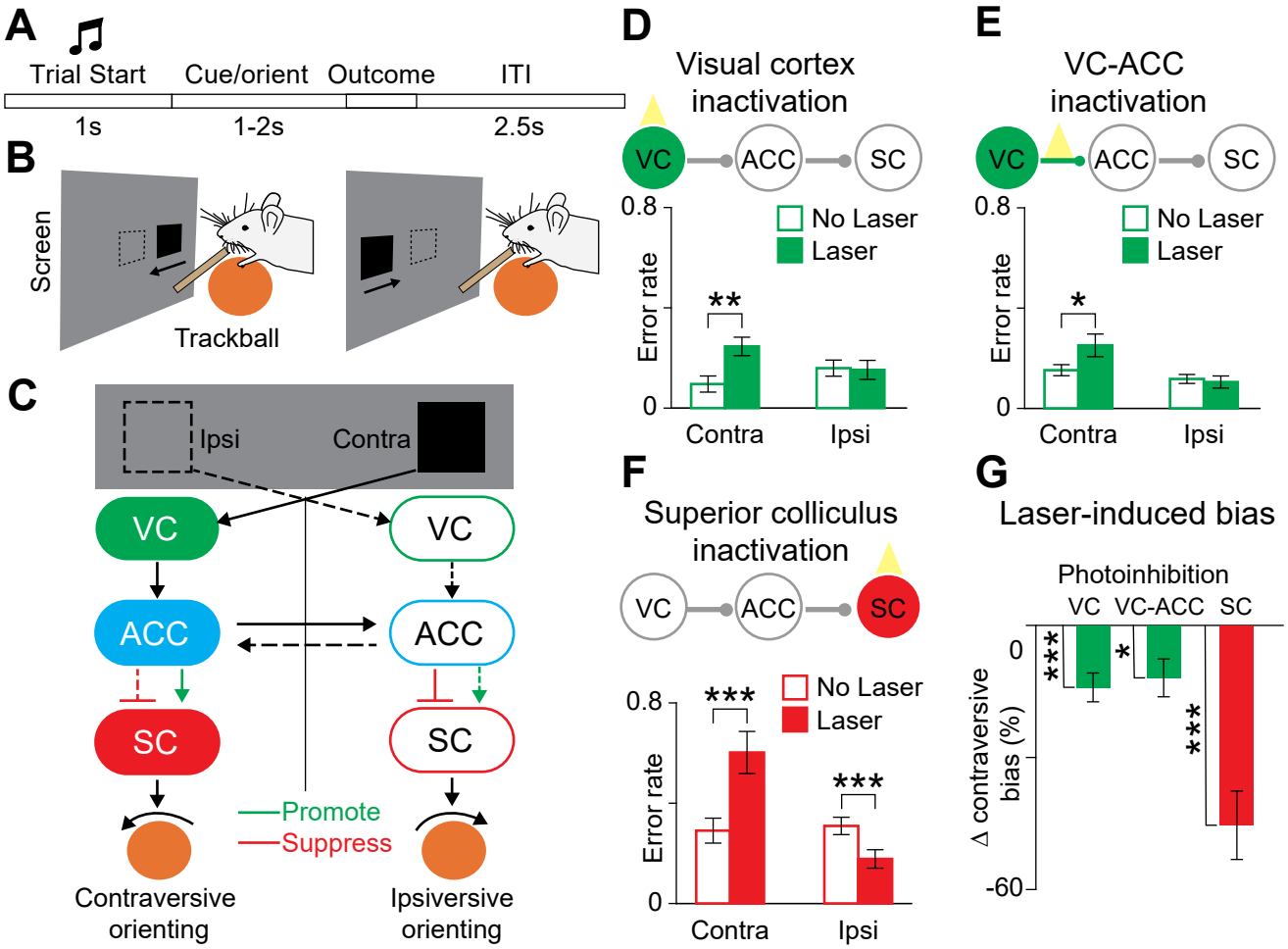

Figure 2. VC, VC inputs to ACC, and SC are necessary for task performance. A) Trial events during the visual forepaw orienting task. B) Schematic showing the behavioral setup. Mice move stimuli presented in either hemifield to the center by rotating a trackball. C) Hypothesis for the role of the ACC in the task. D) Mean error rate on contraversive and ipsiversive trials with (solid) and without (unfilled) VC inactivation (n = 11 sessions, 4 mice). E, F) Similar to C, except for inactivation of VC-ACC axons (n = 11 sessions, 4 mice) and the SC (n = 10 sessions, 5 mice), respectively. G) Normalized laser-induced change in contraversive bias (proportion of trials with a contraversive movement out of all completed trials) with photoinactivation is shown. *p < 0.025, **p < 0.01, ***p < 0.005 (Wilcoxon signed-rank test). Significance evaluated at Bonferroni-adjusted p-value of 0.025.

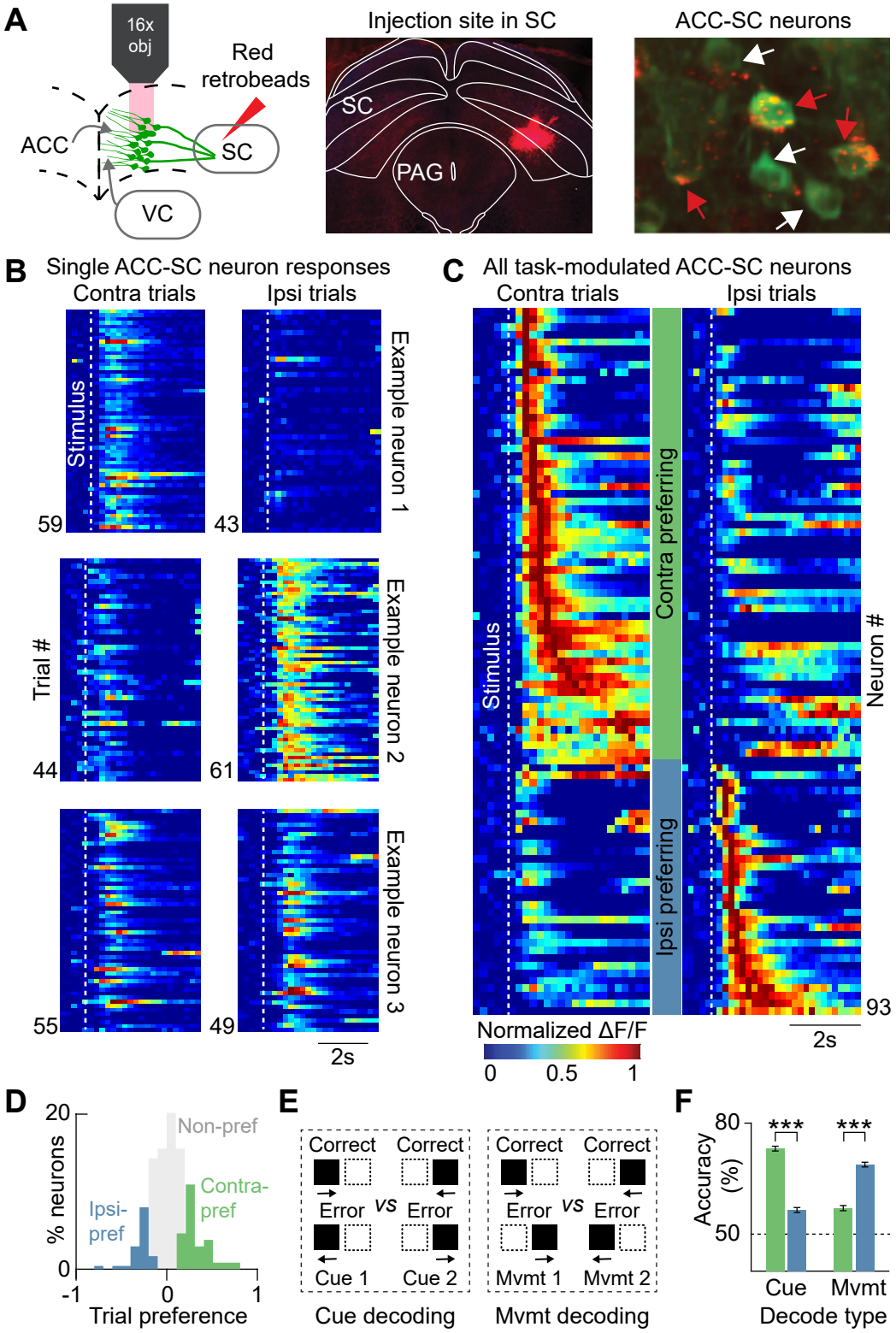

Figure 3. Task-responses of ACC-SC neurons. A) GCaMP6s-imaging of layer 5 during the task. ACC-SC were identified by injecting red retrobeads in SC_m. Recordings were made from 1572 neurons in five expert mice (12 behavioral sessions, 2-3 sessions per animal), of which 416 were ACC-SC neurons. B) Single-trial responses of three representative ACC-SC neurons on correct contra- and ipsiversive trials. C) Session- averaged task-responses of individual ACC-SC neurons (rows). Responses are grouped by trial preference and sorted within each group by the time of peak response. Color bar applies to all color plots. D) Distribution of trial preference scores for task-modulated ACC-SC neurons. E) Combination of correct and error trials used for decoding cue or movement information. F) Predictive accuracy of cue or movement decoders trained with the activity of contra- or ipsiversive-preferring ACC-SC neurons. ***$p < 10^{-5}$; Wilcoxon rank-sum test. Error bars are 95% bootstrap confidence intervals. Significance evaluated at Bonferroni-adjusted p-value of 10^{-5}.

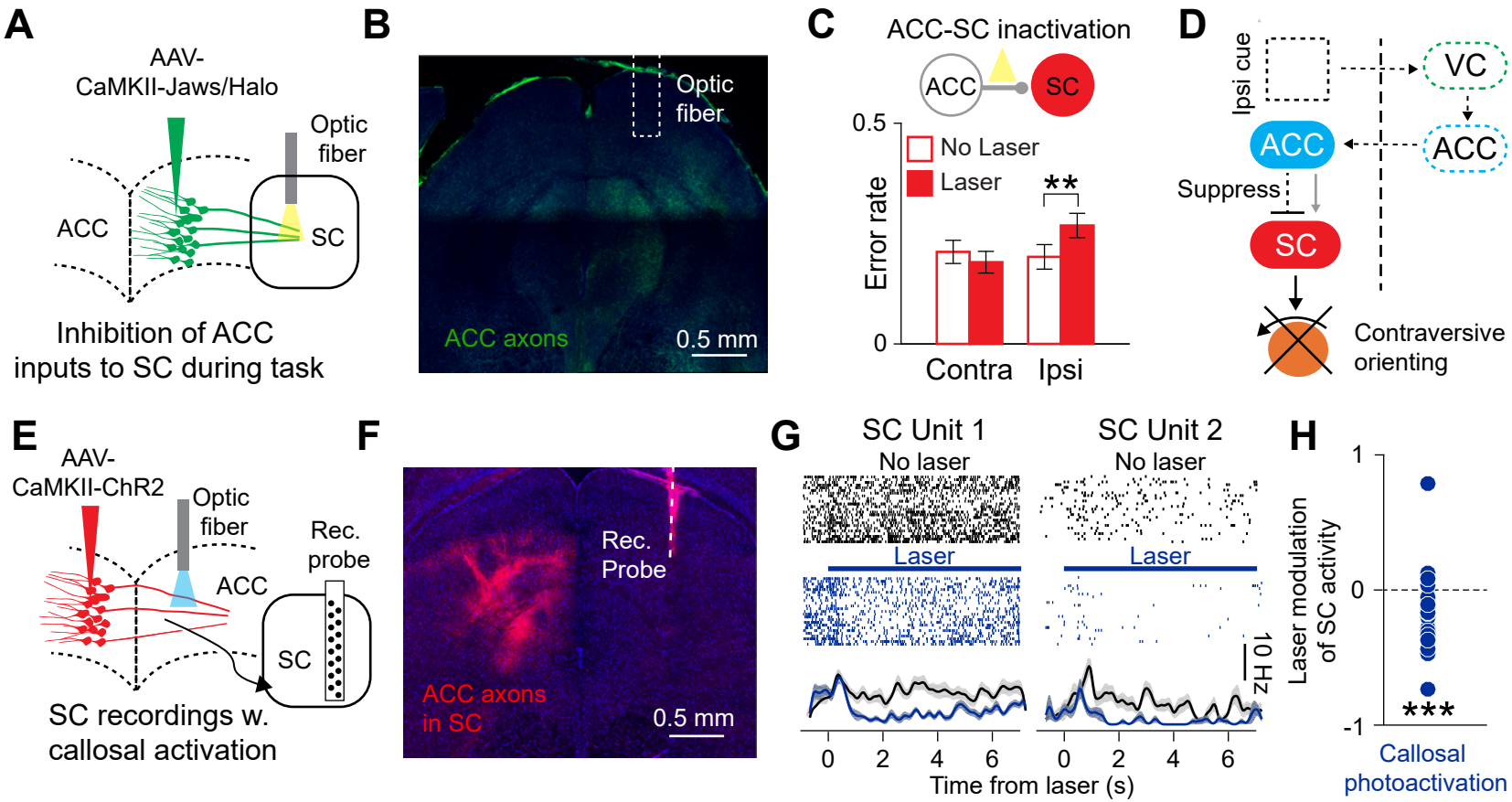

Figure 4. ACC outputs to SC_m suppress incorrect contraversive orienting. A) Inactivation of CaMKII-Jaws-GFP or CaMKII-eNpHR3.0-GFP (Halo) expressing ACC axons in SC_m with orange light (593 nm) during the task. B) Halo-GFP expressing axons in SC_m, along with the optic fiber track. C) Mean error rate on contra- and ipsiversive trials with and without laser inactivation of ACC outputs to SC_m (n = 20 sessions, 7 mice). D) Model summarizing results from this experiment. E) AAV virus encoding CaMKII-ChR2-mCherry was injected unilaterally in the ACC and an optic fiber was implanted in the opposite hemisphere. Extracellular recording probe was inserted on the same side as the optic fiber in the SC. F) ChR2-mCherry expressing ACC axons in the SC_m and recording probe track. G) Spontaneous activity of two example SC units with and without photostimulation of callosal axons. H) Laser- modulation indices of single SC_m units with photostimulation of callosal axons. **$p < 0.01$, ***$p < 0.005$ (Wilcoxon signed-rank test).

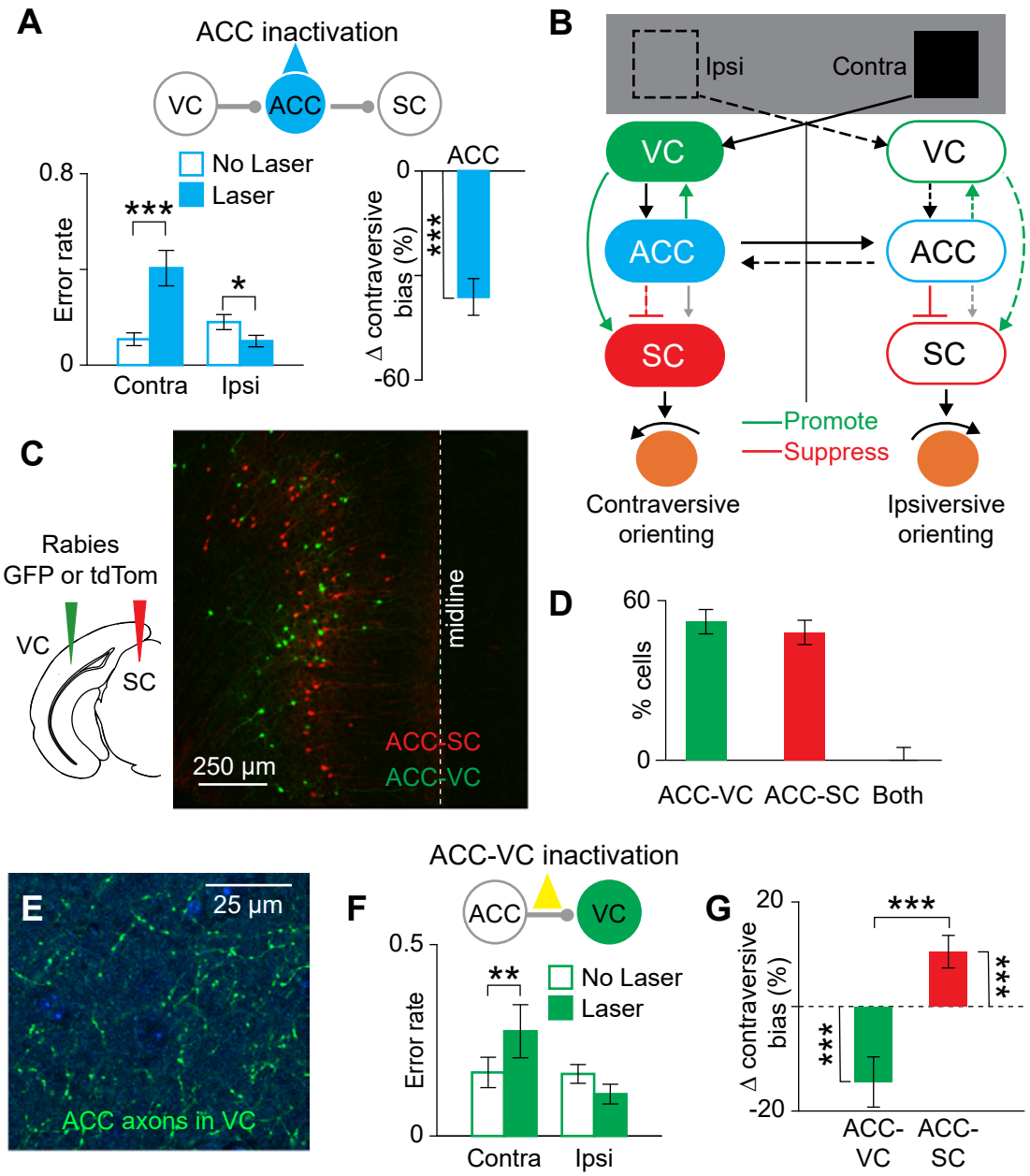

Figure 5. ACC outputs to the VC promote correct contraversive orienting. A) Mean error rates on contraversive and ipsiversive trials with (solid) and without (unfilled) ACC inactivation (n = 14 sessions, 5 mice). Normalized laser-induced change in contraversive orienting bias with inactivation of ACC is shown on right. B) Circuit model for bilateral control of orienting by distinct ACC outputs. C) Dual- color retrograde tracing from VC and SC_m. Back-labeled ACC neurons projecting to SC_m (red) or VC (green). D) Proportion of back-labeled neurons projecting to either or both areas (n = 3 animals). E) ACC was injected with an AAV virus expressing CaMKII-Jaws-GFP and its outputs to the VC were inactivated with orange light through a chronic window. F) Error rates for contraversive and ipsiversive trials with (filled) and without (unfilled) photoinhibition of ACC outputs to the VC (n = 12 sessions, 4 mice). G) Comparison of normalized laser-induced change in contraversive bias for inactivation of ACC outputs to VC (green) or SC_m (red). *$p < 0.025$, **$p < 0.01$, ***$p < 0.005$ (Wilcoxon signed rank or rank sum test). Significance evaluated at Bonferroni-adjusted p-value of 0.025.

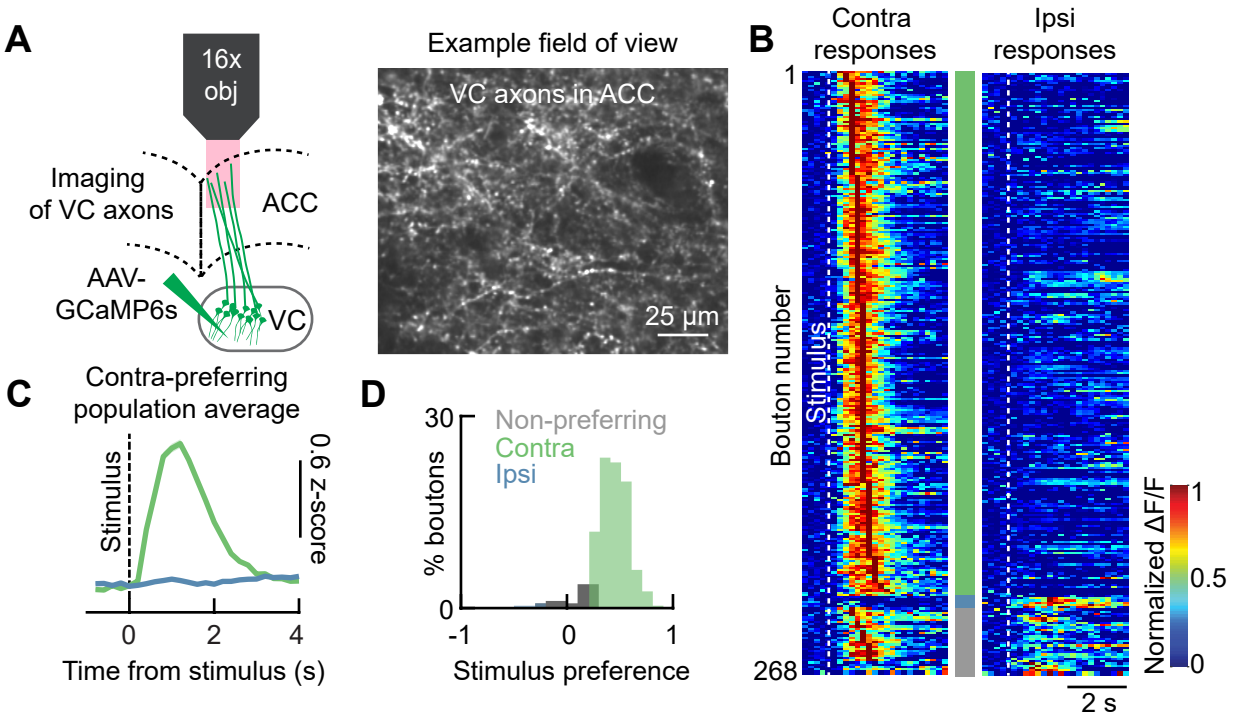

Extended Data Figure 1. Visually-evoked responses of VC inputs to the ACC. A) Two-photon imaging of GCaMP6s-expressing VC axons in the ACC. B) Session-averaged responses of individual visually-responsive boutons to stimuli presented in hemifield contra- or ipsilateral to the recording site (black square, ~20º size, 1s). Responses are grouped by their stimulus preference (contralateral, green; ipsilateral, blue, non-preferring, gray) and sorted within each group by their peak response time. C) Population-averaged response of contra-preferring boutons to contralateral (green) and ipsilateral (blue) stimuli. D) AUROC analysis was used to calculate a stimulus preference score for each visually-responsive bouton. This score ranges from -1 (ipsi selective) to 1 (contra selective). Distribution of scores for 268 visually-responsive VC boutons in ACC from 4 mice is shown.

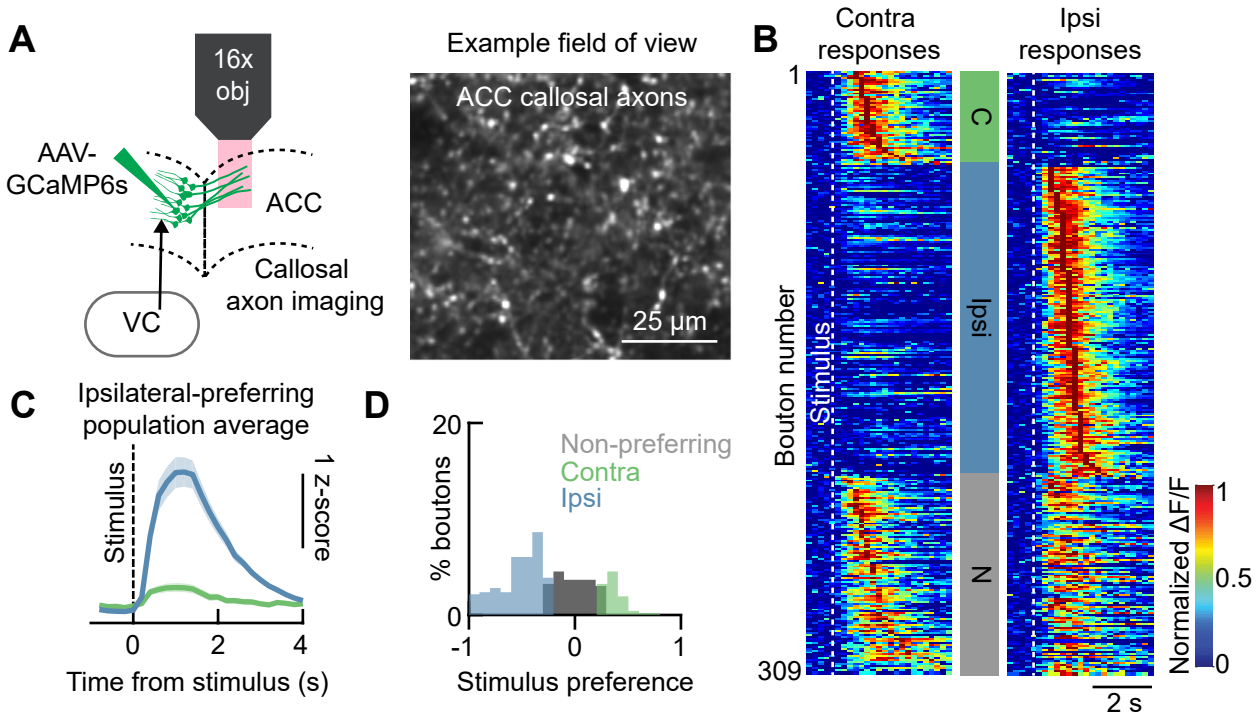

Extended Data Figure 2. Visually-evoked responses of ACC callosal axons. A) Left, ACC was injected with an AAV virus expressing GCaMP6s and labeled axons were imaged through a chronic window over the opposite ACC. Right, Example field of view of GCaMP6s- expressing axons and boutons imaged in vivo. B) Color map of session-averaged responses of individual visually-responsive boutons to stimuli presented contralateral or ipsilateral to the recording site (1s duration, 20º size, sinusoidal drifting grating). Responses are grouped by their stimulus preference (C, contra; N; non- preferring) and sorted within each group by their peak response time. C) Population-averaged response of ipsilateral-preferring boutons to contralateral (green) and ipsilateral (blue) stimuli. D) Histogram showing the distribution of stimulus preference scores for all visually-responsive callosal boutons (n = 309 boutons from 5 mice).

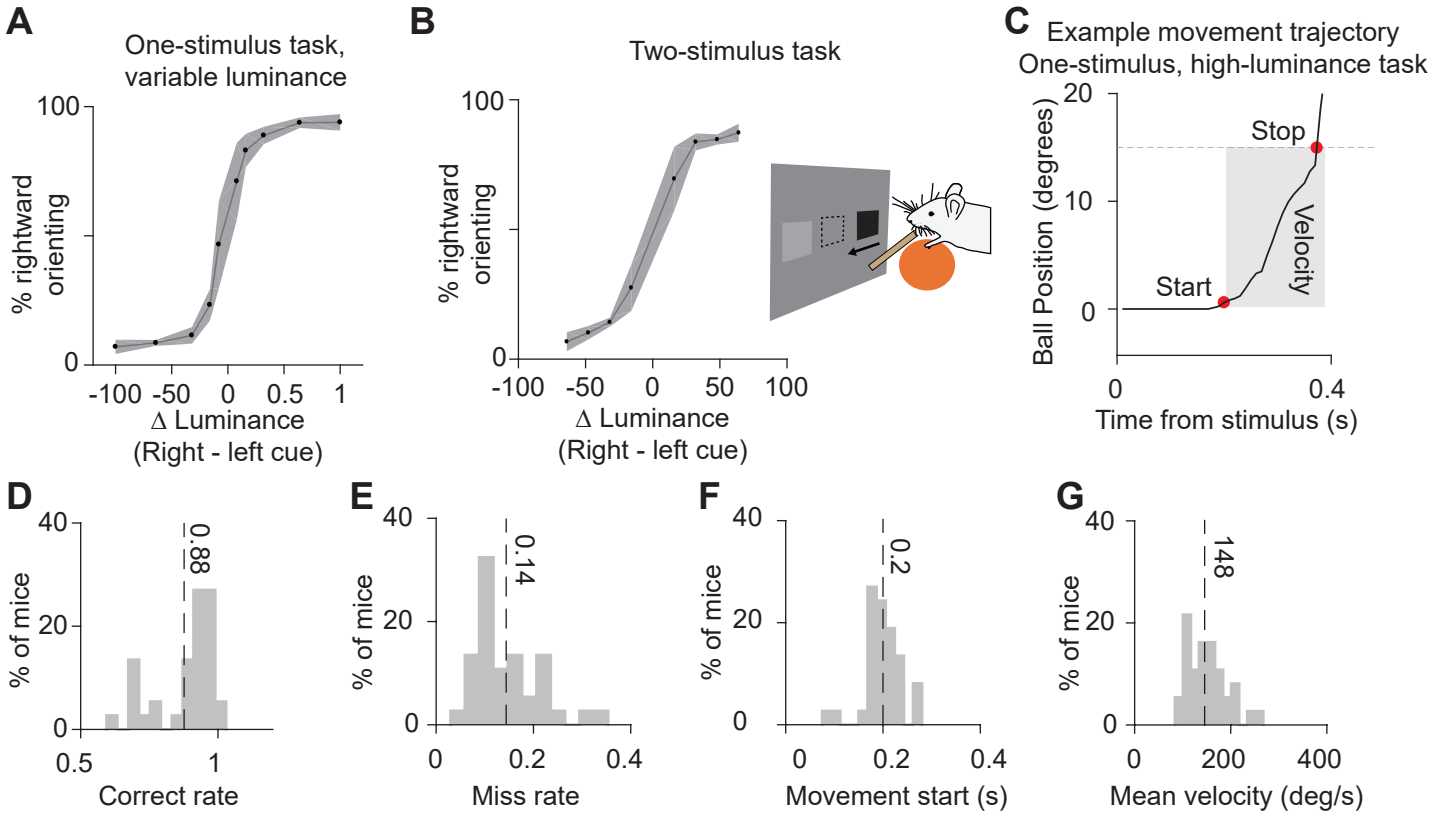

Extended Data Figure 3. Performance on the behavioral task. A) Psychometric curve showing performance on the task with stimuli of varying luminance (n = 3-6 mice for each luminance). B) Psychometric performance on two-stimulus variant of the task (n = 3-5 mice for each luminance pair). C) Example movement trajectory trace. Kinematic analysis was used to detect the movement start time. Average instantaneous movement velocity was calculated between movement start time and the time at which the ball position reached the threshold (dotted line). D-G) Probability distributions for correct rate, miss rate, movement start time, and mean instantaneous movement velocity across a cohort of mice (n = 37 mice). Mean values are shown with dotted vertical lines.

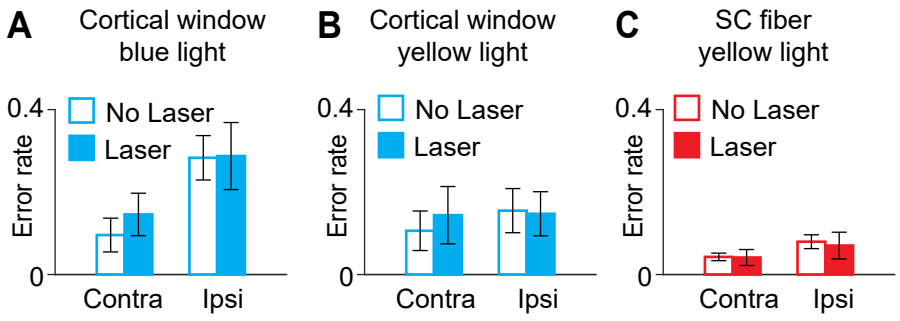

Extended Data Figure 4. Light delivery in the absence of opsins does not affect behavioral performance. A, B) Mice were implanted with a chronic window over the ACC. No opsin-expressing viruses were injected on the side that was targeted with blue or yellow light (20mW). Mean error rate on contraversive and ipsiversive trials with and without laser is shown. C) Same as A, B, except yellow light was delivered to SC_m through an implanted fiber optic cannula.

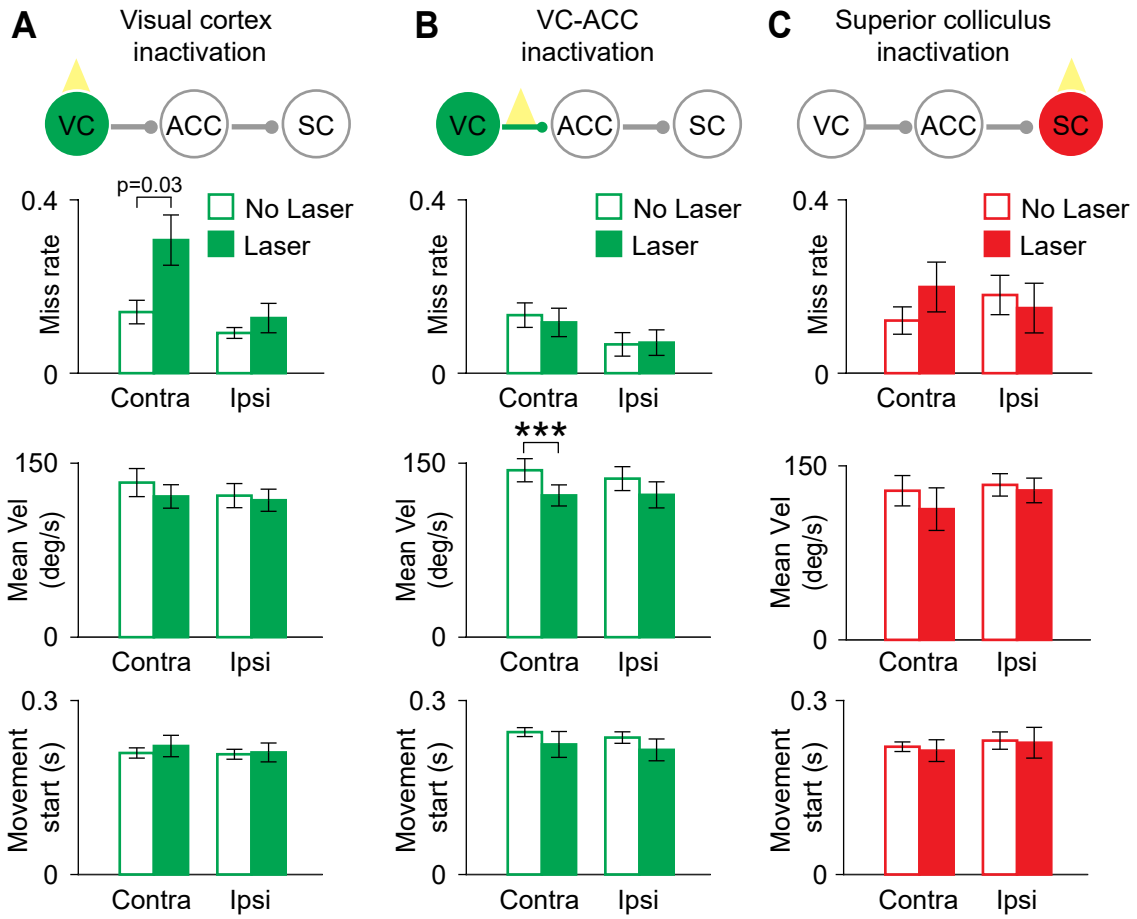

460 **Extended Data Figure 5. Effect of photoinhibition of VC, VC inputs to ACC, and SC_m on**
461 **the miss rate and movement metrics.** A) Jaws-expressing neurons in the visual cortex were
462 inactivated on a random subset of trials with orange light (593 nm) delivered through a chronic
463 window. Mean miss rate, movement velocity, and movement start time on contraversive and
464 ipsiversive trials with (solid) and without (unfilled) VC inactivation (n = 15 sessions, 5 mice). B,
465 C) Similar as in A, except for inactivation of VC-ACC pathway (n = 11 sessions, 4 mice)
466 and of SC_m (n = 11 sessions, 5 mice). Jaws-expressing VC axons in ACC were inhibited by
467 delivering yellow light through a chronic window. SC_m was inhibited by delivering yellow light
468 onto Jaws expressing neurons through an implanted fiber. ***$p < 0.005$, Wilcoxon signed-rank
469 test. Significance evaluated at Bonferroni-adjusted p-value of 0.025.

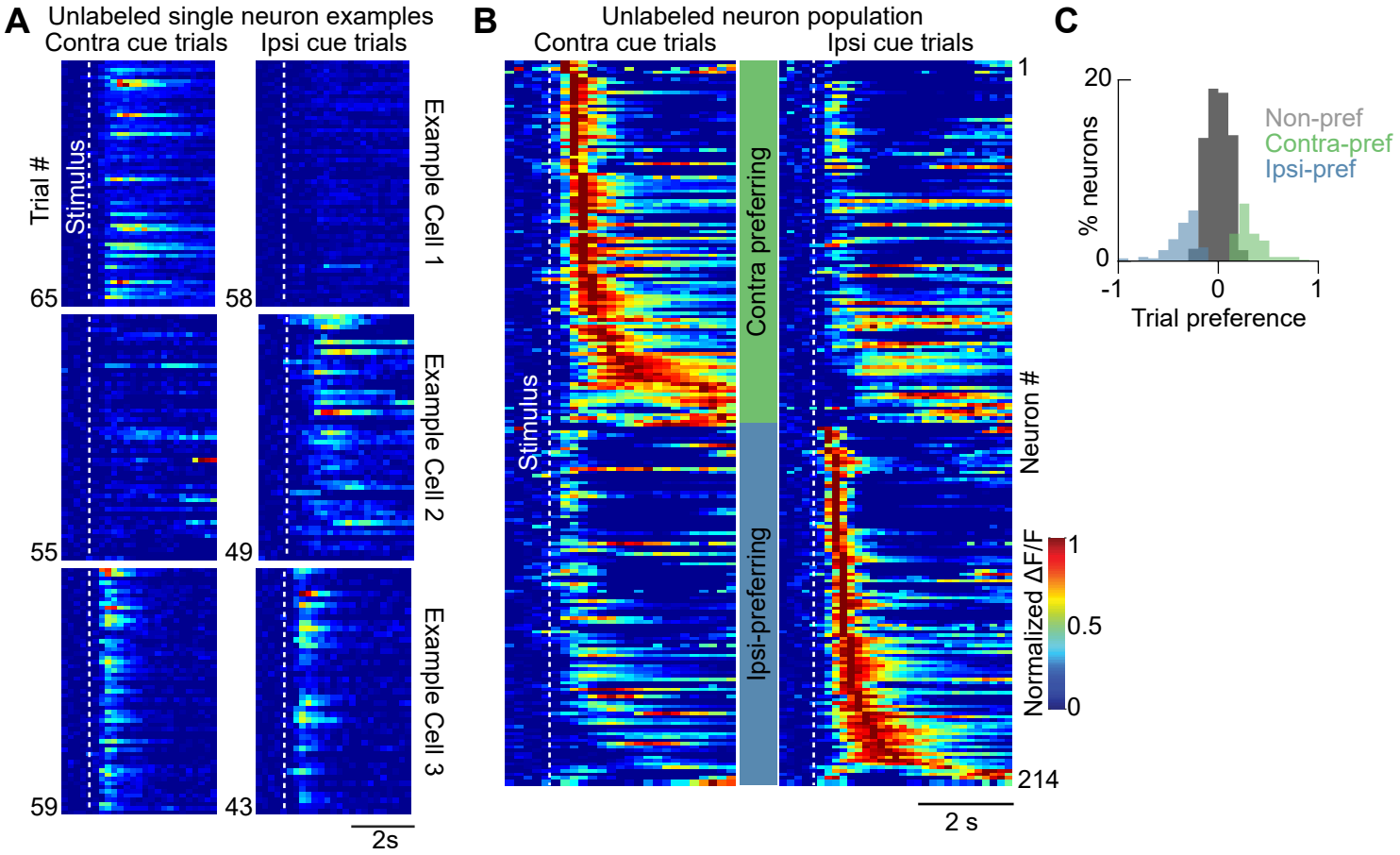

Extended Data Figure 6. Calcium responses of non-SC projecting ACC neurons during the task. A) Task- responses of three unlabeled ACC neurons on correct contraversive and ipsiversive trials. B) Color map showing session-averaged responses of individual task-modulated non-SC projecting neurons (rows) on the indicated correct trials. Responses are grouped by trial preference and sorted within each group by the time of peak response. Stimulus onset is denoted by the white dotted line. Color bar also applies to B. C) Distribution of trial preference scores for task-modulated non-SC projecting neurons.

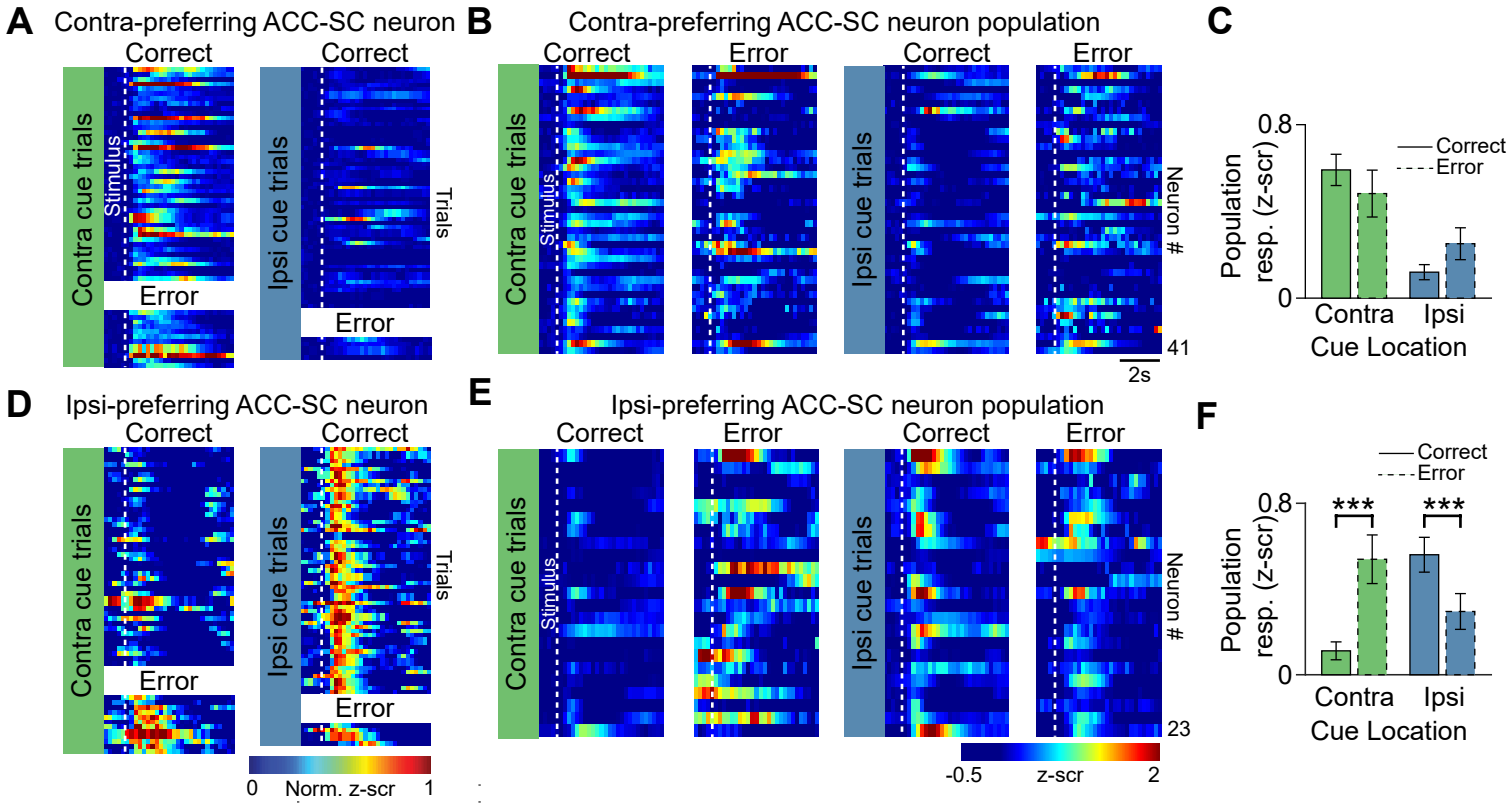

Extended Data Figure 7. Error modulation of ACC-SC task-responses. A) Single-trial responses (rows) of an example contra-preferring ACC-SC neuron on correct and error trials. B) Session-averaged responses of single contra-preferring ACC-SC neurons (rows) on correct and error trials. Neurons are sorted by their trial preference score. Only sessions with at least 5 trials in each condition are included. C) Population activity (averaged over 1s after stimulus onset) of contra-preferring ACC-SC neurons on correct (solid) and error (dotted) contraversive (green) or ipsiversive (blue) cue trials. D-F) Same as A-C, except for ipsiversive-preferring neurons. Scale bars shown in D and E also applies to A and B, respectively. ***$p < 0.005$; Wilcoxon signed-rank test. Significance evaluated at Bonferroni-adjusted p-value of 0.025.

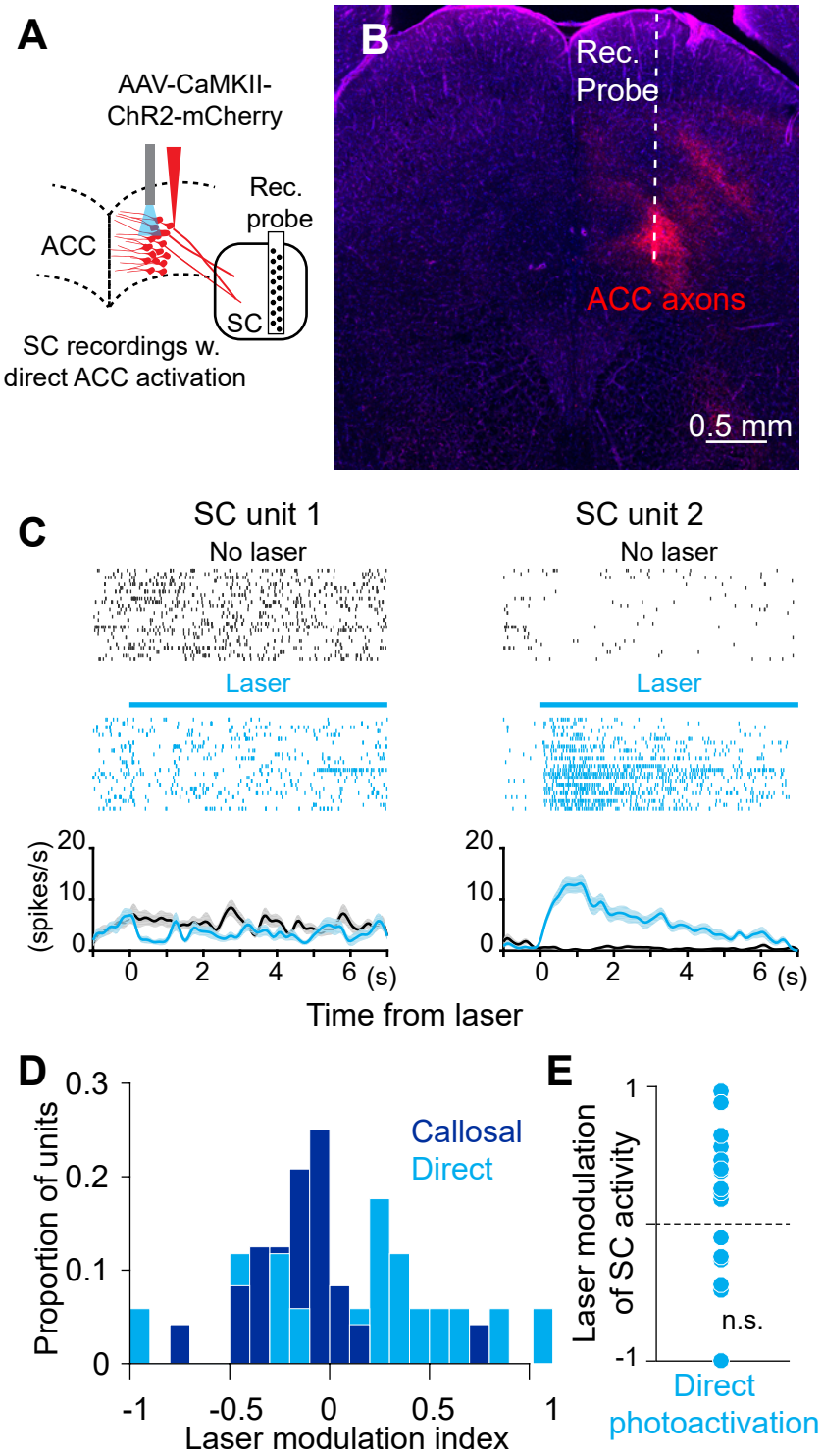

Extended Data Figure 8. Effect of direct optogenetic activation of ACC neurons on single-unit activity in the SCm. A) An AAV virus encoding CaMKII-ChR2-mCherry was injected in the ACC and an optic fiber was implanted on the same side. Extracellular recording probes were inserted in the SC ipsilateral to the fiber. B) Histological section showing ChR2-expressing ACC axons in the SC. Track made by the recording probe is also shown. C) Activity of two example single-units recorded in the SC with (blue) and without (black) optogenetic activation of the ACC. D) Histogram depicting laser-modulation indices for single SC units with photoactivation of callosal inputs and of cell bodies in the ACC. Only cells significantly modulated by laser activation are included in this analysis. E) Laser-modulation indices of single SC units with direct photostimulation of cell bodies in the ACC.

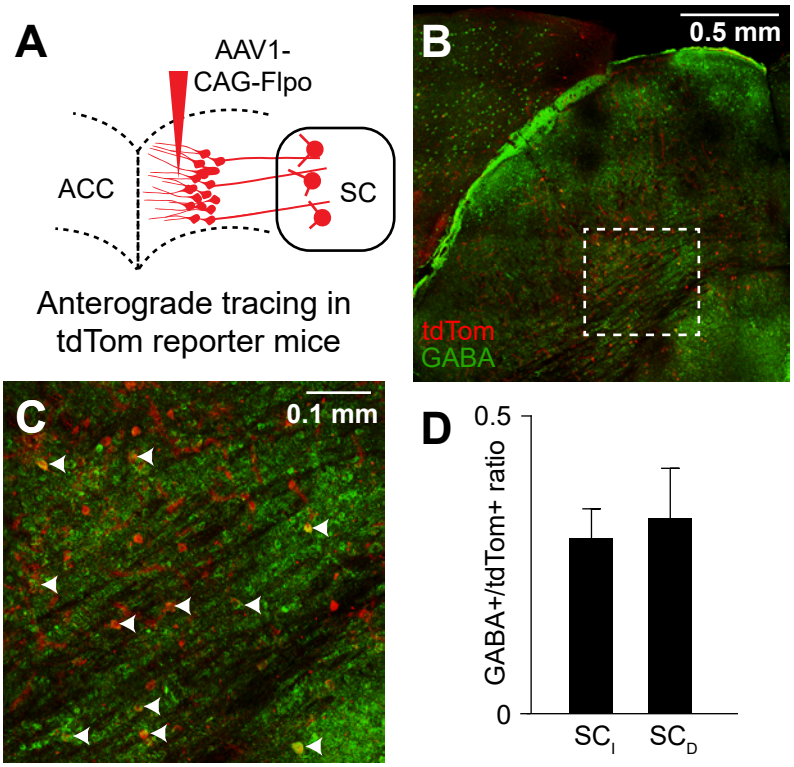

Extended Data Figure 9. Anterograde labeling of SC neurons targeted by ACC outputs. A) Anterograde tracing of ACC outputs to the SC using AAV1 viruses. B) Anterogradely labeled tdTomato-expressing (red) and GABA-containing neurons (green). C) Higher magnification image of the area bounded by dotted white square in B. Arrowheads mark neurons double-labeled for tdTomato and GABA. D) Proportion of tdTomato-expressing SC neurons co-labeled with GABA in intermediate (SC_i) and deep layers (SC_d).

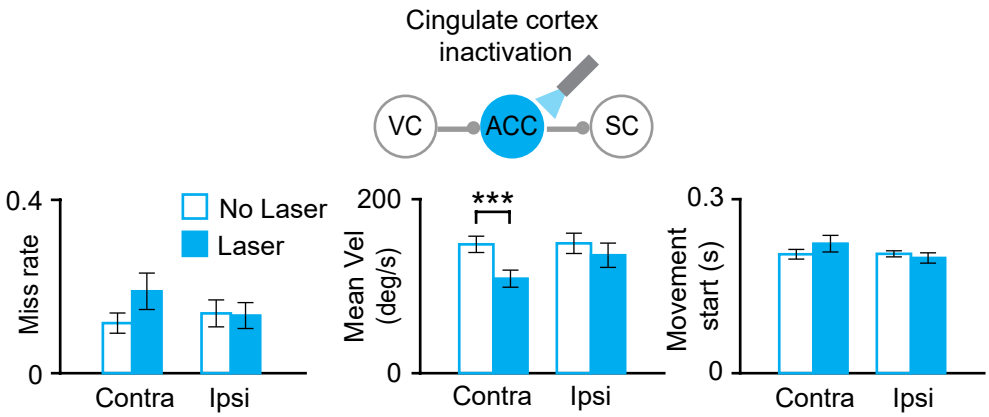

Extended Data Figure 10. Effect of photoinhibition of the ACC on movement metrics. Effect of inactivation on the miss rate, movement start time, and mean instantaneous velocity (n = 14 sessions, 5 mice). ACC was inactivated by photostimulating ChR2-expessing local inhibitory neurons with blue light (473 nm). ***$p < 0.005$ (Wilcoxon signed-rank test). Significance evaluated at Bonferroni-adjusted p-value of 0.025.

A Model schematic

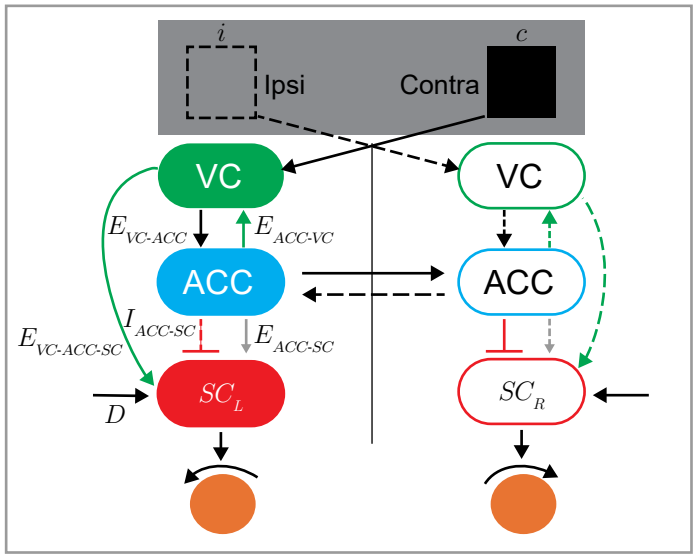

Model →

B Linear model

Activity levels in each SC (SC_L and SC_R) for contraversive trial (c)

$$SC_L(c) = c \cdot E_{ACC\text{-}SC} - (1-c) \cdot I_{ACC\text{-}SC} + c \cdot E_{ACC\text{-}VC\text{-}SC} + D$$
$$SC_R(c) = (1-c) \cdot E_{ACC\text{-}SC} - c \cdot I_{ACC\text{-}SC} + (1-c) \cdot E_{ACC\text{-}VC\text{-}SC} + D \qquad \text{(eq. 1)}$$

Behavioral performance on contraversive and ipsiversive trials given by:

$$SC_L(c) - SC_R(c)$$
$$SC_R(i) - SC_L(i) \qquad \text{(eq. 2)}$$

Model perturbation ↓

C

For each unilateral optogenetic experiment, set corresponding pathway variables to 0. For example, ACC inactivation on a contra trial yields:

$$SC_L(c) = c \cdot \cancel{E}_{ACC\text{-}SC} - (1-c) \cdot \cancel{I}_{ACC\text{-}SC} + c \cdot \cancel{E}_{ACC\text{-}VC\text{-}SC} + D$$
$$SC_R(c) = (1-c) \cdot E_{ACC\text{-}SC} - c \cdot \cancel{I}_{ACC\text{-}SC} + (1-c) \cdot E_{ACC\text{-}VC\text{-}SC} + D \qquad \text{(eq. 3)}$$

$\begin{bmatrix} SC_L(c) - SC_R(c) \\ SC_R(i) - SC_L(i) \end{bmatrix}$ for control and three optogenetic experiments:

$$\begin{array}{c} \text{Control} \\ \hline \text{ACC-SC} \\ \hline \text{ACC} \\ \hline \text{SC} \end{array} \begin{bmatrix} 2c-1 & 2c-1 & 2c-1 & 0 \\ -(2i-1) & -(2i-1) & -(2i-1) & 0 \\ -(1-c) & c & 2c-1 & 0 \\ 1-i & -i & -(2i-1) & 0 \\ -(1-c) & 0 & -(1-c) & 0 \\ 1-i & 0 & 1-i & 0 \\ -(1-c) & c & -(1-c) & -1 \\ 1-i & -i & 1-i & -1 \end{bmatrix} \begin{bmatrix} E_{ACC\text{-}SC} \\ I_{ACC\text{-}SC} \\ E_{ACC\text{-}VC\text{-}SC} \\ D \end{bmatrix} = b$$

Matrix A — Unknown variables x — Behavioral performance

$$Ax = b \qquad \text{(eq. 4)}$$

Estimate $\hat{x}_j$ from each opto expt. →

D Use $\hat{x}_j$ to simulate ACC-VC inactivation

$$P\hat{x}_j = b_{ACC\text{-}VC},$$
$$\text{where } P = \begin{bmatrix} SC_L(c) - SC_R(c) \\ SC_R(i) - SC_L(i) \end{bmatrix}$$
with $E_{ACC\text{-}VC\text{-}SC}$ set to 0 (eq. 5)

Prediction of behavioral deficit with ACC-VC inactivation ↓

E

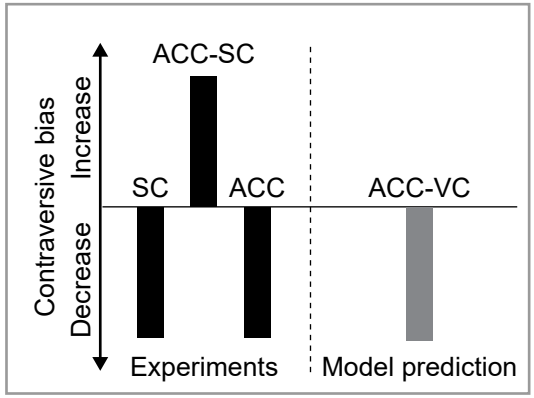

Extended Data Figure 11

Extended Data Figure 11. Linear activity model for predicting the effect of inactivation of ACC outputs to the VC. A) An anatomically-inspired linear activity model was used to predict the contribution of ACC-VC to orienting in the task (see Methods for complete details). The schematic assumes that the left side of the brain was inactivated and accordingly designates stimuli as contralateral or ipsilateral. Activity in SC_L (i.e., left SC_m) and SC_R was expressed as the linear sum of activity from four excitatory input pathways: 1) direct ACC-SC pathway that excites the SC on contraversive trials ($E_{ACC\text{-}SC}$), 2) direct ACC-SC pathway that inhibits the SC on ipsiversive trials ($I_{ACC\text{-}SC}$), 3) ACC-VC pathway that excites the SC on contraversive trials ($E_{ACC\text{-}VC\text{-}SC}$), and 4) a pathway representing the baseline, task-independent activity of the SC (D). B) Equations relating contributions of these pathways to activity in the two SC_m hemispheres (SC_L, SC_R). We parameterized the contribution of the ACC-SC and ACC-VC-SC pathways by variables c and i representing the observed proportion of ACC-SC neurons preferentially active on contraversive and ipsiversive trials, respectively ($c = 0.65$ and $i = 0.35$; see Methods). Each trial type is described by two equations that express activity in SC_L and SC_R on that trial; eq. 1 shows a pair of example equations for a contraversive trial. We assume that contraversive (or ipsiversive) movements result when $SC_L - SC_R > 0$ (or $SC_L - SC_R < 0$) for a given trial (eq. 2). C) We derived a qualitative estimate (see below) for the contribution of each of the four inputs to activity in SC_m by using the average behavioral performance from control conditions and three crucial inactivation experiments (of the ACC, SC or ACC-SC). Optogenetic inactivation is represented in the model by setting the contribution of the corresponding pathway(s) to 0. Eq. 3 illustrates the representation of unilateral inactivation of the left ACC on a contraversive trial. Three of the four input pathways are dependent on the ACC and are set to 0 (red strikethroughs) for the SC_L equation. Note that the inhibitory $I_{ACC\text{-}SC}$ pathway in the right ACC is zeroed because it relies on callosal inputs from left ACC, which is inactivated in this example. Eq. 4 shows these equations derived in a similar way for control and optogenetic inactivation of the ACC, SC, and ACC outputs to the SC, and expressed in matrix form, for contraversive trials. Each pair of rows corresponds to a specific experiment, wherein the first row is $SC_L - SC_R$ (as described for eq. 2) for contra and the second row for ipsi trials (Matrix A). The unknown variables are in vector x, and the observed behavioral performance for contralateral and ipsilateral stimulus trials for each experiment is given by vector b. Generically, this relationship is expressed as $Ax = b$. Determining the contribution of each pathway to the difference in activity between the two SC_m hemispheres, and hence contraversive or ipsiversive orienting, requires solving for the unknown variables in vector x. We derived an estimate for this vector, termed $\hat{x}_j$, using a common linear algebra technique (least-squares approximation) from each of the three optogenetic experiments (denoted by the subscript j; see Methods). Note that $\hat{x}_j$ estimates the contribution of the ACC-VC pathway ($E_{ACC\text{-}VC\text{-}SC}$), but the behavioral results from its optogenetic inactivation were not included in the derivation of $\hat{x}_j$. D) We simulated inactivation of the ACC-VC pathway on the left side by setting $E_{ACC\text{-}VC\text{-}SC}$ to 0 and derived an equation for the difference in activity between the two SC_m hemispheres ($SC_L - SC_R$) for contralateral and ipsilateral trials (eq. 5), similar to that done for deriving matrix A in eq. 3. Multiplying this matrix P by $\hat{x}_j$ gave three predictions of behavioral results expected from inactivation of ACC-VC pathway, one from each of the three optogenetic experiments considered in the model. E) Schematic summary of behavioral results observed with inactivation of the SC, ACC, and ACC-SC pathway. The model predicts that inactivation ACC-VC pathway decreases contraversive orienting.

Methods

Detailed Methods are included at the end of the document.

References

1. Frank, M. J., Doll, B. B., Oas-Terpstra, J. & Moreno, F. Prefrontal and striatal dopaminergic genes predict individual differences in exploration and exploitation. *Nat. Neurosci.* **12,** 1062–8 (2009).
2. Humphries, M. D., Khamassi, M. & Gurney, K. Dopaminergic Control of the Exploration-Exploitation Trade-Off via the Basal Ganglia. *Front. Neurosci.* **6,** 9 (2012).
3. Blanchard, D. C., Griebel, G. & Blanchard, R. J. Mouse defensive behaviors: pharmacological and behavioral assays for anxiety and panic. *Neurosci. Biobehav. Rev.* **25,** 205–18 (2001).
4. Shenhav, A., Cohen, J. D. & Botvinick, M. M. Dorsal anterior cingulate cortex and the value of control. *Nature Neuroscience* **19,** 1286–1291 (2016).
5. Fadok, J. P. *et al.* A competitive inhibitory circuit for selection of active and passive fear responses. *Nature* **542,** 96–100 (2017).
6. Hardung, S. *et al.* A Functional Gradient in the Rodent Prefrontal Cortex Supports Behavioral Inhibition. *Curr. Biol.* **27,** 549–555 (2017).
7. Miller, E. K. & Cohen, J. D. An integrative theory of prefrontal cortex function. *Annu. Rev. Neurosci.* **24,** 167–202 (2001).
8. Cohen, J. D., McClure, S. M. & Yu, A. J. Should I stay or should I go? How the human brain manages the trade-off between exploitation and exploration. *Philos. Trans. R. Soc. Lond. B. Biol. Sci.* **362,** 933–42 (2007).
9. Wimmer, R. D. *et al.* Thalamic control of sensory selection in divided attention. *Nature* **526,** 705–709 (2015).
10. Moore, T. Control of eye movements and spatial attention. *Proc. Natl. Acad. Sci.* **98,** 1273–1276 (2001).
11. Grunfeld, I. S. & Likhtik, E. Mixed selectivity encoding and action selection in the prefrontal cortex during threat assessment. *Curr. Opin. Neurobiol.* **49,** 108–115 (2018).
12. Bukalo, O. *et al.* Prefrontal inputs to the amygdala instruct fear extinction memory formation. *Sci. Adv.* **1,** e1500251 (2015).
13. Rozeske, R. R. *et al.* Prefrontal-Periaqueductal Gray-Projecting Neurons Mediate Context Fear Discrimination. *Neuron* **97,** 898–910 (2018).
14. Otis, J. M. *et al.* Prefrontal cortex output circuits guide reward seeking through divergent cue encoding. *Nature* **543,** 103–107 (2017).
15. Kim, C. K. *et al.* Molecular and Circuit-Dynamical Identification of Top-Down Neural Mechanisms for Restraint of Reward Seeking. *Cell* **170,** 1013–1027 (2017).

16. Ferenczi, E. A. *et al.* Prefrontal cortical regulation of brainwide circuit dynamics and reward-related behavior. *Science* **351,** aac9698 (2016).
17. Murugan, M. *et al.* Combined Social and Spatial Coding in a Descending Projection from the Prefrontal Cortex. *Cell* **171,** 1663–1677 (2017).
18. Pinto, L. & Dan, Y. Cell-Type-Specific Activity in Prefrontal Cortex during Goal-Directed Behavior. *Neuron* **87,** 437–50 (2015).
19. Goard, M. J., Pho, G. N., Woodson, J. & Sur, M. Distinct roles of visual, parietal, and frontal motor cortices in memory-guided sensorimotor decisions. *Elife* **5,** 4841–4843 (2016).
20. Li, N., Chen, T.-W., Guo, Z. V., Gerfen, C. R. & Svoboda, K. A motor cortex circuit for motor planning and movement. *Nature* **519,** 51–56 (2015).
21. Britten, K. H., Shadlen, M. N., Newsome, W. T. & Movshon, J. A. The analysis of visual motion: a comparison of neuronal and psychophysical performance. *J. Neurosci.* **12,** 4745–65 (1992).
22. Erlich, J. C., Bialek, M. & Brody, C. D. A cortical substrate for memory-guided orienting in the rat. *Neuron* **72,** 330–343 (2011).
23. Burgess, C. P. *et al.* High-Yield Methods for Accurate Two-Alternative Visual Psychophysics in Head-Fixed Mice. *Cell Rep.* **20,** 2513–2524 (2017).
24. Raposo, D., Kaufman, M. T. & Churchland, A. K. A category-free neural population supports evolving demands during decision-making. *Nat. Neurosci.* **17,** 1784–1792 (2014).
25. Harvey, C. D., Coen, P. & Tank, D. W. Choice-specific sequences in parietal cortex during a virtual-navigation decision task. *Nature*. **484**, 62–68 (2012).
26. Felsen, G. & Mainen, Z. F. Midbrain contributions to sensorimotor decision making. *J. Neurophysiol.* **108,** 135–47 (2012).
27. Sanders, J. I. & Kepecs, A. Choice ball: a response interface for two-choice psychometric discrimination in head-fixed mice. *J. Neurophysiol.* **108,** 3416–23 (2012).
28. Munoz, D. P. & Everling, S. Look away: the anti-saccade task and the voluntary control of eye movement. *Nat. Rev. Neurosci.* **5,** 218–28 (2004).
29. Ye, L. *et al.* Wiring and Molecular Features of Prefrontal Ensembles Representing Distinct Experiences. *Cell* **165,** 1776–1788 (2016).
30. Koike, H. *et al.* Chemogenetic Inactivation of Dorsal Anterior Cingulate Cortex Neurons Disrupts Attentional Behavior in Mouse. *Neuropsychopharmacology* **41,** 1014–23 (2016).
31. White, M. G. *et al.* Anterior Cingulate Cortex Input to the Claustrum Is Required for Top-Down Action Control. *Cell Rep.* **22,** 84–95 (2018).
32. Schmitt, L. I. *et al.* Thalamic amplification of cortical connectivity sustains attentional control. *Nature* **545,** 219–223 (2017).
33. Hanks, T. D. *et al.* Distinct relationships of parietal and prefrontal cortices to

evidence accumulation. *Nature* **520,** 220–3 (2015).
34. Schafer, R. J. & Moore, T. Selective attention from voluntary control of neurons in prefrontal cortex. *Science* **332,** 1568–71 (2011).
35. Zhang, S. *et al.* Selective attention. Long-range and local circuits for top-down modulation of visual cortex processing. *Science* **345,** 660–5 (2014).
36. Poort, J. *et al.* Learning Enhances Sensory and Multiple Non-sensory Representations in Primary Visual Cortex. *Neuron* **86,** 1478–90 (2015).
37. Wang, Q. & Burkhalter, A. Area map of mouse visual cortex. *J. Comp. Neurol.* **502,** 339–57 (2007).
38. Hikosaka, O. & Wurtz, R. H. Modification of saccadic eye movements by GABA-related substances. I. Effect of muscimol and bicuculline in monkey superior colliculus. *J. Neurophysiol.* **53,** 266–91 (1985).
39. Hofbauer, A. & Dräger, U. C. Depth segregation of retinal ganglion cells projecting to mouse superior colliculus. *J. Comp. Neurol.* **234,** 465–474 (1985).
40. Svoboda, K. & Li, N. Neural mechanisms of movement planning: motor cortex and beyond. *Current Opinion in Neurobiology* **49,** 33–41 (2018).
41. Felsen, G. & Mainen, Z. F. Neural substrates of sensory-guided locomotor decisions in the rat superior colliculus. *Neuron* **60,** 137–48 (2008).
42. Zingg, B. *et al.* AAV-Mediated Anterograde Transsynaptic Tagging: Mapping Corticocollicular Input-Defined Neural Pathways for Defense Behaviors. *Neuron* **93,** 33–47 (2017).
43. Zhang, S. *et al.* Organization of long-range inputs and outputs of frontal cortex for top-down control. *Nat. Neurosci.* **19,** 1733–1742 (2016).
44. Leinweber, M., Ward, D. R., Sobczak, J. M., Attinger, A. & Keller, G. B. A Sensorimotor Circuit in Mouse Cortex for Visual Flow Predictions. *Neuron* **95,** 1420–1432.e5 (2017).
45. Zhao, X., Liu, M. & Cang, J. Visual cortex modulates the magnitude but not the selectivity of looming-evoked responses in the superior colliculus of awake mice. *Neuron* **84,** 202–213 (2014).
46. Wang, Q. & Burkhalter, A. Stream-related preferences of inputs to the superior colliculus from areas of dorsal and ventral streams of mouse visual cortex. *J. Neurosci.* **33,** 1696–705 (2013).
47. Isa, T. & Saito, Y. The direct visuo-motor pathway in mammalian superior colliculus; novel perspective on the interlaminar connection. *Neurosci. Res.* **41,** 107–113 (2001).
48. Tehovnik, E. J., Slocum, W. M. & Schiller, P. H. Saccadic eye movements evoked by microstimulation of striate cortex. *Eur. J. Neurosci.* **17,** 870–878 (2003).
49. Wallace, S. F., Rosenquist, A. C. & Sprague, J. M. Ibotenic acid lesions of the lateral substantia nigra restore visual orientation behavior in the hemianopic cat. *J. Comp. Neurol.* **296,** 222–252 (1990).

50. Hikosaka, O., Takikawa, Y. & Kawagoe, R. Role of the Basal Ganglia in the Control of Purposive Saccadic Eye Movements. *Physiol. Rev.* **80,** 953–978 (2000).

Acknowledgements: We thank Vincent Pham for technical assistance with histological experiments. This work was supported by: National Eye Institute, F32 EY024857 (R.H.), F32 EY028028 (G.O.S.), R01 EY007023 (M.S.); National Institute of Mental Health, K99 MH112855 (R.H.), U01MH106018 (I.R.W), U01MH109129 (I.R.W.); National Institute of Neurological Disease and Stroke, U01 NS090473 (M.S.); NSERC (V.B.P.); National Science Foundation, EF1451125 (M.S.); Simons Foundation Autism Research Initiative (M.S.).

Author contributions: R.H. and M.S. conceived the project and developed the concepts presented. R.H. designed the experiments and analysis approach with contribution from M.S. R.H. and G.P. designed and implemented the behavioral task. R.H. carried out anatomical, behavioral, optogenetic, and calcium imaging experiments, with contributions from G.O.S. and L.G, and analyzed the data. E.A. developed the linear activity model, with input from R.H. and M.S. V.B.P. performed and analyzed the extracellular recording experiments. I.C.W. provided unpublished reagents. R.H. and M.S. wrote the manuscript with input from all authors.

Competing Interests: The authors declare no competing interests.

Methods

Animals: All experimental procedures performed on mice were approved by the Massachusetts Institute of Technology Animal Care and Use Committee. Mice were housed on 12 hour light/dark cycle. Animals were group housed before surgery and singly housed afterwards. Adult mice (> 2 months) of either sex were used for these studies. In addition to wild type mice, transgenic lines of the following genotypes were used: PV-Cre (Jackson Laboratory stock # 008069), VGAT-ChR2-YFP (Jackson Laboratory stock # 014548), Rbp4-Cre (MMMRC stock # 031125), Ai94(TITL-GCaMP6s)-D (Jackson Laboratory stock # 024104), and Ai65(RCFL-tdT)-D (Jackson Laboratory stock # 021875).

Surgical procedures: Surgeries were performed under isoflurane anesthesia (3-4% induction, 1-2.5% maintenance). Animals were given analgesia (slow release buprenex, 0.1mg/kg and Meloxicam 0.1mg/kg) before surgery and their recovery was monitored daily for 72 hours. Once anesthetized, animals were fixed in a stereotaxic frame. The scalp was sterilized with betadine and ethanol. For anatomical tracing experiments, we made a midline incision in the scalp using a scalpel blade. Depending on the experiment, rabies or AAV viruses were injected in the visual cortex (AP: -3.5mm, ML: 2.5mm, DV: 0.5 mm), caudal ACC (AP: 0.3mm, ML: 0.5mm, DV: 0.5 mm), rostral ACC (AP: 1.6mm, ML: 0.3mm, DV: 1.3 mm), or the superior colliculus (at AP: -3.6mm, ML: 1mm, and DV: 1.5mm) using a microinjector (Stoelting). After virus injection, the scalp was reclosed with sutures and skin adhesive (Vetbond).

The following surgical procedures were performed for optogenetics or imaging experiments. For experiments requiring the use of dental acrylic, we removed a portion of the scalp using spring scissors, scraped away the periosteum membrane overlying the skull, and used a dental drill to abrade the skull to improve adhesion. Same animals were used for inactivation of the visual cortex or its projection to the anterior cingulate cortex. We drilled a 3mm craniotomy over the visual cortex and made 8-12 injections (100nL each) of an AAV5.CaMKII.Jaws-KGC-GFP-ER2 (University of North Carolina vector core) virus 0.5mm below the surface in a grid pattern. Injections were centered on the left primary visual cortex (centered at AP: -3.5mm, ML: 2.5mm; range AP: 4 to 3mm, ML: 2.2

717 to 2.8mm). Craniotomies were fitted with a chronic window, which was assembled from a
718 3mm coverslip attached to a 5mm coverslip (Warner instruments) with UV curing
719 adhesive (Norland 61). Chronic windows were adhered to the skull using Metabond dental
720 acrylic (Parkell). Visual cortex axons in ACC were photoinhibited through 3mm chronic
721 windows implanted over the ACC (centered at AP: 0.5mm and ML: 0mm, n = 2) or through
722 cannulas (300µm/0.39NA core fiber optic coupled to a 2.5mm stainless steel ferrule;
723 CFMC13L02, Thorlabs) with optic fibers extending 0.3mm below the pial surface (n = 2).
724 For photoinhibition of the ACC, we used either VGAT-ChR2 mice (n = 2) or PV-Cre mice
725 (n = 3) injected with AAV1.EF1.dflox.hChR2(H134R)-mCherry (University of
726 Pennsylvania vector core) at coordinates AP: 0.5mm, ML: 0.5mm, and DV: 0.5 and 1mm
727 (250 nL at each site). PV-Cre mice were implanted with cannulas such that the optical
728 fiber was 0.3mm below the pia. Fiber optic cannulas were secured on the skull using
729 layers of Metabond and were protected with a dust cap until used for experiments. VGAT-
730 ChR2 mice were implanted with a 3mm chronic window over the ACC. For photoinhibition
731 of the superior colliculus (SC), we injected AAV5-hSyn.Jaws-KGC-GFP-ER2 (100nL) in
732 the intermediate/motor layer (at AP: -3.6mm, ML: 1mm, and DV: 1.5mm) and implanted
733 a fiber optic cannula 0.2mm dorsal to the injection site in wildtype mice (n = 5). For
734 modulating ACC outputs to the superior colliculus, we injected either AAV5-CaMKII-Jaws-
735 KGC-GFP-ER2 (n = 5), or AAV5-CaMKII-eNpHR3.0-EYFP (n = 2) (University of North
736 Carolina vector core) in the ACC of wildtype mice and implanted a fiber optic cannula
737 over the intermediate layer of the superior colliculus (at AP: -3.6mm, ML: 1mm, DV:
738 1.3mm) on one side of the brain. In a subset of these experiments, AAV5-CaMKII-Jaws-
739 KGC-GFP-ER2 was injected bilaterally in the ACC. One side of the brain was implanted
740 with a chronic window over the visual cortex and the SC on the opposite side was
741 implanted with a fiber optic cannula.

742 For all imaging experiments in the ACC, we drilled a 3mm craniotomy (at same
743 coordinates as used for optogenetic experiments) and implanted a chronic window
744 assembled from two 3mm coverslips glued to a 5mm coverslip using the UV curable
745 adhesive (double-chronic window). The additional 3mm coverslip was required to
746 minimize movement artifacts for GCaMP recordings during task performance. To label
747 superior colliculus-projecting ACC neurons (ACC-SC), we injected 100nL of red

retrobeads (Lumaflour) in the intermediate/motor layer of the SC (at AP: -3.6mm, ML: 1mm, DV: 1.7mm). For axonal imaging experiments, 200nL of AAV1-Syn-GCaMP6-WPRE-SV40 virus was injected unilaterally in the visual cortex (AP: -3.5mm, ML: 2.5 mm, DV: 0.5 mm) or the opposite ACC (AP: 0.5mm, ML: 0.5 mm, DV: 0.5 mm).

To assess the effect of ACC photoactivation on single-unit activity in the SC, 250 nL of AAV5-CaMKII-ChR2 was injected in the ACC at (AP: 0.5mm, ML: 0.5mm, DV: 0.5mm). Depending on the experiment, the fiber optic cannula was implanted either on the same side or opposite to the site of virus injection, with the fiber tip extending 0.3mm below the surface. Stereotaxic location of the SC (AP: -3.6mm, ML: 1mm) was marked on the skull with black ink. The skull was covered with silicone elastomer (Kwik-Cast, World Precision Instruments) to prevent Metabond from adhering to it directly.

For all experiments, after implantation of chronic windows or optic fiber cannulas, the skull was attached to a stainless steel custom-designed head plate (eMachines.com) using Metabond. Animals were allowed to recover for at least five days before commencing water restriction for behavioral experiments.

Virus-mediated anatomical tracing: Standard histological techniques were used for analysis of retrograde and anterograde transsynaptic tracing experiments and for post-hoc verification of implantation/injection sites. Mice were deeply anesthetized with isofluorane and transcardially perfused with a 4% paraformaldehyde (PFA) solution prepared in phosphate buffered saline (PBS). Extracted brains were postfixed in 4% PFA overnight at 4°C, then kept in PBS until sectioning. Fixed brain tissue was sectioned using a microtome (Leica VT-1000) into coronal slices (thickness of 50-100 µm, depending on the experiment). Slices were stained with DAPI and mounted on glass microslides using Vectashield hardset mounting media. Mounted sections were stored at 4°C until they were imaged using a laser scanning confocal microscope (Leica SP8).

Rabies viral vectors were made as described[51]. Briefly, HEK 293T cells (ATCC CRL-11268) were transfected with expression vectors for the ribozyme-flanked viral genome (cSPBN-4GFP (Addgene 52487) or pRVΔG-4tdTomato (Addgene 52500)), rabies viral genes (pCAG-B19N (Addgene 59924), pCAG-B19P (Addgene 59925), pCAG-B19G (Addgene 59921), and pCAG-B19L (Addgene 59922)), and the T7 polymerase (pCAG-T7Pol (Addgene 59926)). Supernatants were collected from 4 to 7

779 days after transfection, filtered, and pooled, passaged 3-4 times on BHK-B19G2 cells[52]
780 at a multiplicity of infection of 2-5, then passaged on BHK-EnvA2 cells[52] at a multiplicity
781 of infection of 2. Purification, concentration, and titering were done as described.

782 To make AAV1-CAG-Flpo, the Flpo gene[53] was cloned into pAAV-CAG-FLEX-
783 EGFP (Addgene 59331) to make pAAV-CAG-Flpo. Serotype 1 AAV was produced by
784 triple transfection of HEK 293T cells with pAAV-syn-Flpo, pAAV-RC1, and pHelper
785 (Cellbiolabs VPK-401) (per 15 cm plate, 15.5 ug, 21.0 ug, and 33.4 ug respectively) using
786 Xfect (Clontech 631318) transfection reagent. Supernatants and cells were harvested at
787 72 hours posttransfection and viruses purified and concentrated by iodixanol gradient
788 centrifugation[54].

789 For quantification of dual-rabies retrograde tracing experiments from caudal and
790 rostral ACC, we sliced the brain into 100 μm section and imaged GFP and/or tdTomato
791 fluorescence from every other slice using a 10x/0.4NA objective (Leica). Anatomical
792 landmarks, such as position/size of ventricles, corpus callosum, striatum, and
793 hippocampus, were used to manually align slices to a standard mouse brain atlas[55]. Back-
794 labeled cells were counted using the cell counter plugin in ImageJ (NIH). For the results
795 presented in Fig. 1C, we counted the number of retrogradely neurons present in the
796 different divisions of the visual cortex and normalized by the total number of GFP- and
797 tdTomato-expressing back-labeled cells found in the posterior cortex (0 to -4.0 mm
798 posterior, relative to Bregma). For quantifying the distribution of cells projecting to the
799 intermediate and deep layers of the SC (Fig. 1J), we counted the number of cells found
800 in the ACC as a function of distance from Bregma in 0.5mm bins. Since the sensory and
801 intermediate/motor layers of the superior colliculus are <0.5mm apart, it is challenging to
802 restrict virus injection to the motor layer. However, the frontal cortex predominantly
803 projects only to the motor layer; hence, to minimize contamination from virus spillover into
804 the sensory layer of the superior colliculus, we normalized the number of neurons in the
805 ACC by the total number of back-labeled neurons found in the frontal cortex (0 to +3mm
806 anterior, relative to Bregma).

807 We injected rabies viruses encoding GFP or tdTomato into the visual cortex or the
808 superior colliculus to identify ACC neurons projecting to these structures. We counted the
809 total number of back-labeled neurons in the ACC (AP range 0 to 1mm), every 200 μm in

each animal and quantified the proportion of neurons that were labeled with GFP, tdTomato, or both out of all labeled cells.

We performed anterograde transsynaptic tracing experiments[42] to identify SC neurons that receive inputs from the ACC. We produced the Flp-dependent tdTomato reporter line Ai65F by crossing the Cre- and Flp- dependent tdTomato double-reporter line Ai65D[56] (Jackson Laboratory 021875) to the Cre deleter line Meox2-Cre[57] (Jackson Laboratory 003755), so that only Flp is required for expression of tdTomato. An AAV1-CAG-Flpo virus was injected in the ACC of these mice to label postsynaptic neurons with tdTomato. After allowing 4-6 weeks for tdTomato expression, we sectioned the brain into 50µm slices and used standard immunohistochemistry techniques to identify GABA-expressing neurons co-labeled with tdTomato. The tissue was placed in 5% normal goat serum, 1% triton blocking solution in 0.1M phosphate buffered saline (PBS) for 1 hour at room temperature. It was then incubated in primary antibody against GABA (rabbit anti-GABA, 1:500, A2052 Sigma) and 1% NGS/ 0.5% triton overnight at 4ºC. Following washing in 0.1M PBS 3x10', the tissue was incubated in secondary antibody (goat anti-rabbit IgG AlexaFluor 488, 1:500, Invitrogen) and 1% NGS for 4 hours at room temperature. Tissue was then washed 3x10' in PBS, mounted, and coverslipped with anti-fade mounting medium (Prolong Gold, ThermoFisher). Tiled z-stacks were collected on a confocal microscope (SP8, Leica) using a 20x objective at 1024x1024 resolution, 2 µm apart (~20 z-slices) from sections containing the SC (between -3.4 and -4.7 AP from bregma). We counted the total number of tdTomato-labeled cells in the SC and quantified the proportion of these neurons that were also positive for GABA (Cell counter plugin).

Behavioral apparatus and training: Mice were trained to report the spatial location of visual stimuli by rotating a trackball left or right with their forepaws, similar to a previously described design[27]. Animals were headfixed on a behavior rig assembled from optical hardware (Thorlabs), placed in a polypropylene tube to limit body movement, and positioned ~8 cm from an LCD screen (7" diagonal; 700YV, Xenarc Direct) such that their forepaws rest on a trackball. Ball movements were monitored with a commercially available USB optical trackball mouse (Kensington Expert Mouse K64325). The original trackball was replaced with a 55mm diameter ping pong ball (Joola), which was light enough for mice to rotate comfortably. We inserted a hypodermic tube down the center

841 of the trackball so it could only be rotated along a single axis (left or right). To fix the ping
842 pong ball to the optical mouse, we made grooves in the trackball chassis and secured the
843 hypodermic needle with hot glue. A USB host shield (SainSmart) was used to connect
844 the output of the optical mouse to a microcontroller (Arduino), which ran a custom routine
845 that detected ball movements every 10ms. In the event of a ball movement, the
846 microcontroller outputted a timestamp and the amount of movement (in pixels) to a
847 behavioral control computer running Windows XP (Dell). In addition, a time stamp was
848 sent every 100ms to synchronize timing between the microcontroller and the behavior
849 computer. In our system, one pixel of optical mouse movement corresponded to ~0.15º
850 movement on the ball. Behavioral control was implemented with custom software written
851 in MATLAB (Mathworks) using the Psyhcophysics and the Data Acquistion toolboxes. On
852 each trial, the presented visual cue (black square, ~20º) started on either the left or the
853 right side of the LCD screen. The trackball controlled the location of the visual stimulus in
854 closed-loop in real-time. The gain of coupling between the trackball and the stimulus was
855 calibrated so that rotating the ball by the threshold amount (15º) in the correct direction
856 moved the stimulus from its starting position to the center of the screen. Ball positions
857 were accumulated throughout the trial until the stimulus reached the center or the
858 response window expired. Under this closed-loop control, any movement in the incorrect
859 direction displaced the stimulus farther away from the center and towards the edge of the
860 screen. Hence, such movements had to be offset by additional movement in the correct
861 direction for the stimulus to move to the center of the screen and for the trial to be
862 considered correct. If the ball was moved opposite to the direction of the instructed cue
863 by the threshold amount, the stimulus moved to the edge of screen and the trial was
864 considered incorrect. Water reward was delivered through a metal spout placed within
865 the reach of the tongue on correct trials; the amount dispensed was controlled by opening
866 a solenoid valve for a calibrated period of time.

867 Mice were taken through successive stages of training until they became proficient
868 at the task. Once mice recovered from the surgery, they were water restricted for 5-7 days
869 (≥ 1ml/day) and then trained to lick the metal spout to obtain small water rewards (3-6
870 μL). If mice did not receive their water allotment during training, they were given the
871 remaining amount as hydrogel (Clear H_2O) in their home cage. After mice reliably licked

872 the water spout, they earned water rewards by using the trackball to move the presented
873 stimulus to the center of the screen. To discourage spontaneous trackball movements,
874 mice were required to hold the ball still for 1s to trigger trial start, which was signaled with
875 an auditory tone (0.5s, 1 KHz); the visual cue appeared with a 1s delay after trial start.
876 During early stages of training, only movements in the correct direction contributed to
877 movement of the stimulus. Once mice reliably moved the ball in either direction on >90%
878 of trials, this condition was removed and the movement of the stimulus was fully coupled
879 to the movement of the trackball. In the next stage of training, we used an anti-bias
880 algorithm in which the same stimulus was repeated on consecutive trials if mice made an
881 error until they performed the trial correctly; stimulus location on trials following correct
882 trials were randomly chosen. Once performance reached 70%, the anti-bias algorithm
883 was turned off and stimuli were presented in a randomized manner. Throughout all
884 stages, white noise was used to signal miss trials if mice failed to move the ball to
885 threshold before expiration of the response window. As mice progressed through the
886 training stages, we gradually decreased the response time from 10s to 1-2s. Correct and
887 incorrect trials were signaled with an auditory tone (0.2 kHz and 10kHz, respectively),
888 followed by an inter-trial delay of 2.5s. In a subset of mice, incorrect trials were punished
889 with a brief timeout (3s), lengthening the inter-trial delay to 5.5s.

890 Animals trained for two-photon imaging experiments were taken through two
891 additional stages of training. First, we turned off the closed-loop coupling between the
892 trackball and the stimulus, and flashed stimuli for 100-200ms. Second, we introduced
893 uncertainty in temporal expectancy for stimulus onset by randomizing the period
894 (exponential distribution with mean of ~1.8 seconds, min and max delay of 1 and 5s,
895 respectively) between the auditory cue signaling trial start and the onset of the visual
896 stimulus. Once animals achieved criterion performance of 70% correct with randomized
897 trials, we commenced optogenetic or imaging experiments.

898 We also trained a subset of mice on two variants of the task to interrogate their
899 psychometric performance. In the first variant, we presented a single visual cue as before
900 but of varying luminance values. In the second variant, mice were presented with two
901 cues simultaneous (target and distractor). The luminance of the target cue was set to 64%
902 while that of the distractor cue ranged from 0 to 48%; animals were rewarded for orienting

to the target cue. We quantified performance (excluding miss trials) for each target-distractor stimulus pair to assess the effect of perceptual ambiguity on orienting responses.

Behavioral analysis: We computed several metrics to quantify performance for each trial type on individual behavioral sessions. The error rate was the proportion of trials in which the ball was moved opposite the direction instructed by the cue out of all completed trials for each visual stimulus (i.e., excluding miss trials). The miss rate was the proportion of trials in which the ball was not moved to threshold out of all trials where a given stimulus was presented. The response window was set to 1s for most animals. However, imposing this restriction on some mice led to a high miss rate and a response window of 2s was used instead. The movement start time and movement velocity was calculated using kinematic analysis of movement trajectories. The microcontroller counted the number of pixels the ball was moved in each 10ms time bin. A trace of ball position vs. time from stimulus onset was constructed by taking a cumulative sum of these pixel counts and scaling by 0.15º/pixel. The resulting trace was resampled at 100Hz using the 'interp1' function in MATLAB. Next, we computed instantaneous velocity and acceleration traces by computing the first and second time derivatives of the position trace. Movement start was defined as the first time point when the absolute value of the instantaneous acceleration exceeded a threshold value and the absolute value of the ball position was greater than 0.75º. The acceleration threshold value was optimized manually so that the algorithm picked start times preceding smooth and continuous movements, ignored spurious movements, and performed well across different animals. Robustness of this kinematic analysis was verified by visual inspection of position traces marked with the movement start times picked by the algorithm. Mean instantaneous velocity for each trial was then calculated by averaging the instantaneous velocity values between the movement start time and the time at which the ball position reached the threshold.

Optogenetic manipulation of behavior: Photostimulation was provided with a solid state 473nm blue laser for experiments using ChR2 and a 593nm orange laser for experiments using Jaws or eNpHR3.0 (OptoEngine). Laser stimulation was triggered from the behavior control computer and lasted from 0.3s before to 1s after visual cue onset.

933 15-20% of trials were pseudorandomly selected for photostimulation. We additionally
934 imposed the condition that photostimulation could not occur on two consecutive trials.
935 The output of the laser was coupled to a 300µm core/0.39NA patch cable (Thorlabs) with
936 a FC/PC fiber coupler (OptoEngine). Laser power through the patch cable was measured
937 with a digital power meter before each experiment (Thorlabs). In experiments requiring
938 photostimulation through chronic windows over the visual cortex, the ceramic ferrule of
939 the patch cable was positioned so it filled the entire 3mm window and delivered a constant
940 light pulse with 20mW of power. Since the ACC is a midline structure and the chronic
941 window was implanted such that it exposed both hemispheres, we placed a light
942 obstructing material (Mounting Putty, Scotch) over one hemisphere and positioned the
943 patch cable ferrule so it illuminated a ~1mm spot over the targeted hemisphere. In
944 experiments requiring light delivery through implanted optical fiber, the ceramic ferrule of
945 the patch cable was coupled to the fiber optic cannula with a ferrule mating sleeve
946 (ADAF1, Thorlabs). Constant blue (10-20mW) or yellow (20mW) light was used for
947 photostimulation of inhibitory neurons or visual cortex axons in the ACC, respectively.
948 Activity in the superior colliculus was inhibited by delivering 5-10mW of constant yellow
949 light. Photoinhibition of ACC outputs was achieved by constant yellow light (20mW)
950 illumination through an implanted fiber optic cannula (SC) or through a chronic window
951 (VC).

952 Trials were labeled as ipsiversive or contraversive depending on the location of the
953 presented cue relative to the site of photostimulation. For each experiment, we analyzed
954 the first three sessions with photostimulation in which the performance on non-laser trials
955 for both trial-types was at least 60% correct. In each session, we computed the error rate
956 and the miss rate on ipsiversive and contraversive trials separately for laser and non-
957 laser trials. The effect of photostimulation on behavioral performance was quantified by
958 comparing the error rate between laser-on and laser-off conditions. We similarly
959 quantified the effect of photostimulation on movement start times and movement velocity.

960 We computed contraversive bias as the percentage of trials in which the animal
961 made contraversive movements out of all completed trials (i.e., excluding miss trials)
962 regardless of the stimulus presented. Although stimulus presentations were randomized,
963 individual sessions could have uneven number of contralateral and ipsilateral stimulus

trials. Moreover, the miss rate for the two trial types may not necessarily be the same. To account for these issues, we subsampled the choices made on non-miss contralateral or ipsilateral stimulus trials (5 trials each) and calculated the proportion of trials in which the animal made a contraversive orienting movement separately for laser and non-laser trials. This process was repeated 1000 times for each session. The contraversive bias rate for laser and non-laser trials on each session was then estimated by averaging these 1000 values. The effect of photostimulation was determined by calculating the laser-induced normalized change in contraversive bias using the following equation:

$$\frac{ContraBias_{laser} - ContraBias_{nonlaser}}{ContraBias_{nonlaser}}$$

This value reflects the degree to which photostimulation changes the contraversive bias relative to performance on non-laser trials.

Population statistics were derived by pooling individual sessions across all animals and comparisons were made using the Wilcoxon signed-rank test (two-sided). Since analyses that compared the effect of photostimulation on contraversive and ipsiversive trials tested two hypotheses, we determined significance using the Bonferroni adjusted p-value of 0.05/2 = 0.025. We also used the signed-rank test to determine if the laser-induced normalized change in contraversive bias was from different from zero.

Two-photon microscopy: GCaMP6s fluorescence was imaged through a 16x/0.8 NA objective (Nikon) using galvo-galvo scanning with a Prairie Ultima IV two-photon microscopy system. Excitation light at 910nm was provided by a tunable Ti:Sapphire laser (Mai-Tai eHP, Spectra-Physics) equipped with dispersion compensation (DeepSee, Spectra-Physics). Emitted light was collected with GaAsP photomultiplier tubes (Hamamatsu). A blackout curtain attached to a custom stainless steel plate (eMachineShop.com) was mounted on the headplate to prevent light from the LCD screen from entering the PMTs. Layer 5 GCaMP6s-expressing neurons in transgenic animals were imaged with 2x optical zoom, 350-550μm below the brain surface for 20-minute-long behavioral sessions. Upon completion, excitation wavelength was changed to 830nm, which produced both a signal from the retrobeads and a structural green signal from GCaMP6. Emission signals were split with a dichroic mirror (FF649-Di01; Semrock) mounted in a filter cube and directed to two different PMTs. Simultaneous imaging of both

signals with 830nm excitation facilitated spatial alignment of retrobead signals to GCaMP6s signals collected during behavior and allowed us to identify SC-projecting ACC neurons (see *Image analysis*). 4x optical zoom was used for imaging callosal or visual cortex axons in the ACC up to 100µm below the surface. All imaging experiments were performed at a frame rate of 5Hz. Laser power at the specimen was controlled with pockel cells and ranged from 10 to 50 mW, depending on GCaMP6 expression levels and depth.

Image analysis: Images were acquired using the PrairieView software (Bruker) and saved as multipage TIFF files. Image processing and region of interest (ROI) selection was performed in ImageJ (NIH). To correct for lateralized movements in the x-y axis, images were realigned to a reference frame (the pixel-wise mean of all frames) using the template matching plugin[58]. ROIs were drawn manually over visually identified neurons on reference frames generated by taking the pixel-wise maximum, mean, and standard deviation of all frames. For each neuron, the same shaped ROI was also placed in an adjacent area devoid of other neurons to estimate the background neuropil signal. To minimize the contribution of the neuropil signal to the somatic signal, corrected neuronal fluorescence time series was estimated as $F(t) = F_{raw_soma}(t) – 0.7 \times F_{raw_neuropil}(t)$[59]. Similar image analysis was used for axonal imaging experiments, except ROIs were drawn over visually-identified boutons and fluorescence signals were not adjusted for neuropil contamination. ΔF/F (DFF) for each neuron or bouton was calculated as $\Delta F/F(t) = 100 \times (F(t) – F_0)/F_0$, where F_0 was the estimated mode of the distribution of raw fluorescence values.

To identify retrobead-containing neurons, a reference frame was generated by taking the pixel-wise mean of realigned GCaMP6s frames acquired during the behavioral session. The green channel acquired with excitation at 830nm was realigned to this reference using the template matching plugin. The resulting translation values were then applied to the channel containing signals from retrobeads. An average projection was taken after this realignment and superimposed onto the reference frame used for drawing ROIs. Neurons containing retrobeads were then visually identified.

Analysis of task responses of ACC neurons: For imaging experiments, trials were labeled contraversive or ipsiversive depending on the location of the visual cue relative

to the hemisphere imaged. DFF responses on each trial were aligned by stimulus onset and correct contraversive/ipsiversive trials were sorted into separate groups. The mean DFF activity averaged over a 1s pre-stimulus and 1s post-stimulus period was compared using the Wilcoxon signed-rank test. Neurons with significantly higher activity after stimulus onset ($p < 0.05$, one-sided) on either trial type were considered task-modulated.

To facilitate population comparisons, DFF signals were z-score normalized with baseline activity over a 1s pre-stimulus period. AUROC values were computed for each task-modulated neuron by comparing the z-scored activity (averaged over a 1s period after stimulus onset) on correct contraversive and ipsiversive trials. A trial preference score was then computed as 2 x (AUROC – 0.5); this score ranged from 1 (complete contraversive preference) to -1 (complete ipsiversive preference). To determine if individual task-modulated neurons had significant trial preference, scores were recomputed after shuffling trial labels 1000 times. Observed preference scores outside the center 95% of the shuffled distribution were considered significant ($p < 0.05$, two-sided).

We assayed the visual responsiveness of visual cortex or callosal axons in the ACC in animals passively viewing visual stimuli presented at the same locations as during the task (solid black square for visual cortex axons, gratings drifting at 90º for callosal axons; 1s stimulus duration). Visually responsive boutons were identified by comparing pre-stimulus activity averaged over a 1s period to averaged activity 0.6s-1.2s after stimulus onset (two-sided Wilcoxon signed-rank test, $p < 0.01$). Stimulus preference scores for visually-responsive boutons were computed using the AUROC analysis, similarly to that described above.

Cue and movement decoding: We built linear support vector machine (SVM) classifiers using the LIBSVM library for MATLAB[60] to probe whether neuronal responses represent information about the location of the visual cue or the direction of the orienting movement. Selection of the regularization parameter C was performed with a dataset not included in the analysis. We tested a range of values for C and selected the one which gave the best classifier accuracy on an 8-fold cross-validated dataset ($C = 0.4665$). For this procedure, the classifier was trained to distinguish between correct contraversive and ipsiversive trials. Neurons in this dataset were simultaneously recorded; however, we only

included the minimum number of neurons and trials used in the final decoder for the analysis presented here (see below).

We define the term 'information' here operationally as the prediction accuracy of the trained classifiers[61]. We reasoned that neurons that encode cue information would respond similarly on trials in which the same cue is presented regardless of the direction of the orienting movement chosen on that trial. Similarly, a neuron that encodes movement direction would be active on trials in which a particular movement was chosen regardless of the cue presented. Hence, we used a combination of correct and error trials to train classifiers for decoding cue and movement information (see schematic in Fig. 3E). We trained these decoders with responses of each of the following four types of neurons: 1) contra-preferring, unlabeled; 2) contra-preferring, ACC-SC; 3) ipsi-preferring, unlabeled; 4) ipsi-preferring, ACC-SC.

Since we simultaneously recorded only a few cells in each of these groups, we constructed ‘pseudotrials’ by combining neuronal responses recorded across different sessions with at least 5 error trials for each cue type. There was an unequal distribution of neurons across groups. Hence, we used subsampling so that the same number of neurons were used for training each type of classifier (23 neurons, limited by the number of ipsi-preferring ACC-SC neurons). We also had unequal number of trials between conditions and similarly used subsampling to balance trial types (5 trials for each type). To estimate the predictive power of our classifiers, we ran 1000 iterations of cue and movement decoders separately trained with the z-scored activity (averaged over 1s after stimulus onset) of each of the four types of neurons. A random set of neurons and trials were subsampled on each iteration of the model. We minimized model over-fitting by using the cross validation technique (8-fold) to split the data into a training and testing set on each iteration and estimated classifier performance by averaging the prediction accuracy across the 8 splits. By the end of this procedure, we had 1000 prediction accuracies for each cue/movement decoder trained with the activity of the four different neuron types. We used bootstrapping (subsampling with replacement, 1000 iterations) to calculate a 95% confidence interval for the prediction accuracy of each decoder. To determine if individual decoders performed above chance, we used an identical procedure except that we shuffled the labels for the test data. Mean prediction accuracy

(averaged across the 1000 models) derived from correctly labeled test data and falling outside the center 99% of the shuffled distribution were considered significant. To determine if specific neuron types contain different cue and movement information, we compared the corresponding distribution of prediction accuracies using a Wilcoxon rank-sum test[62]. Since this experiment potentially tested 28 different hypotheses (i.e., two types of decoders for four neuron types), we tested significance at the Bonferoni adjusted p-value of 0.01/28 (~10^{-5}).

Electrophysiological recordings in the SC: We tested the effect of photostimulating ChR2-expressing callosal input axons or directly activating ChR2-expressing cell bodies on activity in the SC. One or two days before the experiments, mice were habituated to head-fixation in 1h sessions. On the day of the experiment, mice were anesthetized with isoflurane and the Metabond and silicone elastomer on the skull were removed. The mouse was placed on the stereotaxic frame and a 500 μm diameter craniotomy was performed on top of the recording site (from bregma: -3.6 to -4 mm anteroposterior and 0.8 to 1 mm mediolateral). The dura above the cortex was removed and the craniotomy was protected with saline and a piece of gelfoam. The side of the craniotomy depended on the experiment, but was always made ipsilateral to the ACC hemisphere in which the fiber optic cannula was implanted. The skull was covered again with silicone elastomer and the animal was returned to its home cage to recover from anesthesia for at least 2 hours. After recovery, mice were headfixed and the silicone and gelfoam overlaying the craniotomy was gently removed. 0.9% NaCl solution was used to keep the surface of the brain wet for the duration of the recordings.

After placing the animal in the recording set up, we submerged a reference silver wire in the NaCl solution on the skull surface. The position of the 16-channel silicone probe (A1x16-Poly2-5mm-50s-177-A16, NeuroNexus) was referenced on lambda and the surface of the brain and lowered slowly (1 min per mm) to reach superficial sensory layer of the superior colliculus (~1.3 mm in the ventral axis) using a motorized micromanipulator (MP – 285; Sutter Instrument Company). The extracellular signal was amplified using a 1x gain headstage (model E2a; Plexon) connected to a 50x preamp (PBX-247; Plexon) and digitalized at 50 kHz. The signal was highpass filtered at 300Hz. Once the visual layer of the SC was identified (characterized by strong and reliable visual

1117 responses to drifting gratings and sparse noise), the recording probe was lowered ~400
1118 µm deeper to the motor layer of the SC. For successful recordings, the silicone probe
1119 was gently retracted and the recording tract was marked by re-entering the DiI coated
1120 probe (2 mg/mL – D3911, ThermoFisher Scientific) at the same location. For some
1121 experiments, we were able to record from two locations spaced 500µm apart in the dorsal-
1122 ventral axis. The brain was harvested post-hoc and sectioned to confirm the probe
1123 location and ChR2 expression in the ACC. Spikes were isolated online with amplitude
1124 threshold using Plexon Recorder software, but re-sorted using the MountainSort
1125 automated spike sorting algorithm [63]. Units were curated manually after automatic
1126 detection.

1127 Visual stimuli were presented during recordings in the SC to increase neuronal
1128 responsiveness. Sparse noise on a 3 x 5 grid (square size was the same as used for
1129 behavior experiments) of black and white square on a gray background (50% luminance)
1130 were displayed for 0.1s, followed by a 0.1s gray screen period. Positions were
1131 randomized within each block such that black and white squares were presented once at
1132 each of the 15 positions. The total duration of a block was 6 sec, with 1s inter-block
1133 intervals. Photostimulation of the ACC (10ms blue light pulses at 20 Hz) was performed
1134 on 50% of the blocks and lasted throughout the block.

1135 Since ACC axons in the SC target the intermediate and deep layers, we focused our
1136 analysis on recordings made from these areas. While we observed robust retinotopically
1137 organized visual responses in the superficial layer, we rarely encountered cells in the
1138 deeper layers that responded to the sparse noise stimuli presented at specific locations.
1139 Therefore, recordings from deeper neurons likely reflect ongoing, spontaneous activity
1140 but we cannot rule that the visual stimulation modulated this tonic level of activity. We first
1141 determined if individual neurons were significantly modulated by laser activation of the
1142 ACC by comparing the firing rates (FR) of activity on non-laser and laser trials. For each
1143 modulated neuron, we computed a laser modulation index using the following equation:

1144
$$\frac{FR_{Laser} - FR_{nonlaser}}{FR_{Laser} + FR_{nonlaser}}$$

1145 To test if photostimulation increased or decreased activity in the SC, we tested if the
1146 population laser modulation index was significantly different from zero. We also compared
1147 the laser modulation observed with direct photoactivation of ACC cell bodies or activation

of callosal input axons. All comparisons were made using either two-sided Wilcoxon rank-sum (unpaired) or signed-rank (paired) tests.

Linear activity model: Causal activity manipulation optogenetic experiments aim to understand how specific circuits contribute to behavioral performance, and can be used to formally derive the contributions of distinct pathways to behavior. An anatomically-inspired linear activity model was used to predict how the ACC-VC projection contributes to task performance by modulating activity in SC_m (Extended Data Fig. 11). In this description, we assume that the left side of the brain was inactivated; contralateral/ipsilateral stimuli are designated relative to the inactivated side. Activity in SC_L (the inactivated side) and SC_R was expressed as the linear sum of inputs from four excitatory pathways: 1) direct ACC-SC pathway that excites the SC on contraversive trials ($E_{ACC\text{-}SC}$); 2) direct ACC-SC pathway that inhibits the SC on ipsiversive trials ($I_{ACC\text{-}SC}$); 3) ACC-VC pathway that excites the SC on contraversive trials ($E_{ACC\text{-}VC\text{-}SC}$), and 4) a default pathway representing the baseline, task-independent activity of the SC (D) (Extended Data Fig. 11A). Pathways 1 and 2 are based on our experiments showing that direct or callosal photoactivation in the ACC increases or decreases activity in the SC, respectively (Fig. 4E-H; Extended Data Fig. 8). Pathway 3 is based on previous experiments showing that stimulus-driven activity in the VC is enhanced by inputs from the ACC[43] and that the VC controls the magnitude of sensory responses of neurons in the superficial SC[45]. We included the non-specific input pathway to account for the baseline activity of SC_m driven by diverse inputs.

We parameterized the contribution of the ACC-SC and ACC-VC-SC pathways by variables c *and* i, representing the drive provided by the ACC on contraversive and ipsiversive trials, respectively. We set these variables based on the observed proportion of ACC-SC neurons preferentially active on contraversive and ipsiversive trials, respectively ($c = 0.65$ and $i = 0.35$, Fig. 3D). Importantly, we tested a range of values for these parameters and obtained similar predictions. We defined two equations that express activity in the left and right SC_m for each type of trial (contra or ipsi). Only equations for contra trial are shown as an example, but equations for ipsi trials are defined similarly and obtained by substituting c with i:

$$SC_L(c) = cE_{ACC\text{-}SC} - (1-c)I_{ACC\text{-}SC} + cE_{ACC\text{-}VC\text{-}SC} + D$$

$$SC_R(c) = (1-c)E_{ACC\text{-}SC} - cI_{ACC\text{-}SC} + (1-c)E_{ACC\text{-}VC\text{-}SC} + D$$

We defined x as a column vector containing the contribution of each of the four input pathways to activity in SC_L and SC_R

$$x = \begin{bmatrix} E_{ACC-SC} \\ I_{ACC-SC} \\ E_{ACC-VC} \\ D \end{bmatrix}$$

and expressed the equations in matrix form (example for contraversive trial shown):

$$\begin{bmatrix} SC_L(c) \\ SC_R(c) \end{bmatrix} = \begin{bmatrix} c & -(1-c) & c & 1 \\ 1-c & -c & 1-c & 1 \end{bmatrix} x$$

This matrix determines the activity in each SC in the absence of any optogenetic perturbation. The optogenetic inhibition of specific areas or anatomical projections is modeled by substituting the corresponding terms in the above matrix by zeros (see example in Extended Data Fig. 11B, eq. 3). Matrices for three crucial inactivation experiments considered in the model (of the ACC-SC, ACC, and SC) are given below for contraversive trials. The first and second row in each represents SC_L and SC_R, respectively, for contraversive trials:

$$\text{ACC-SC: } \begin{bmatrix} 0 & 0 & c & 1 \\ 1-c & -c & 1-c & 1 \end{bmatrix}$$

$$\text{ACC: } \begin{bmatrix} 0 & 0 & 0 & 1 \\ 1-c & 0 & 1-c & 1 \end{bmatrix}$$

$$\text{SC: } \begin{bmatrix} 0 & 0 & 0 & 0 \\ 1-c & -c & 1-c & 1 \end{bmatrix}$$

We assume that behavioral performance on each trial-type is given by the differences $SC_L(c) - SC_R(c)$ and $SC_R(i) - SC_L(i)$, respectively, such that the SC_m hemisphere with the higher level of activity leads to its preferred contraversive orienting movement. Each of the three experiments, in addition to the control experiment, then yields two linear functions of x, one for contraversive trials and one for ipsiversive trials, totaling eight functions. We expressed these functions in matrix form to derive an 8-by-4 matrix A (shown in Extended Data Fig. 11C, eq. 4) that multiplied by vector x describes the behavioral performance ($\boldsymbol{b}$) observed during control and optogenetic experiments (i.e., $Ax = \boldsymbol{b}$, Extended Data Fig. 11C).

Our goal in formulating this linear model is to make a prediction about the contribution of the ACC-VC pathway to behavioral performance that is constrained by the behavioral deficits observed by inactivating the ACC, SC, and ACC-SC pathway. The model, described by the relationship $Ax = \boldsymbol{b}$, posits that optogenetic inactivation experiments cause the observed changes in behavioral performance by perturbing activity in SC_m through the four input pathways represented in x. Hence, we can use this relationship to estimate how activity along pathways represented in x must change to cause the observed changes in behavioral performance. Once we obtain an estimate for x, we can simulate the inactivation of any pathway included in the model (such as the ACC-VC pathway, Extended Data Fig 11D, eq. 5) and predict how behavioral performance should change if the pathway is experimentally perturbed (see details below).

In $Ax = \boldsymbol{b}$, the behavioral performance vector $\boldsymbol{b}$ aggregates the performance observed during control and the three inactivation experiments. Using this aggregate vector provides only a single estimate of x. In contrast, decomposing $\boldsymbol{b}$ into its four components (represented by b_j, three of which correspond to the change in behavioral performance caused by the inactivation experiments) would allow us to derive separate estimates of x (x_j) from each experiment. These estimates can then be used to make three predictions for how inactivating the ACC-VC pathway will change behavioral performance. We reasoned that comparing predictions derived from separately estimated x_j would allow us to determine their robustness, which would not be possible if we derive only a single estimate by using the non-decomposed vector $\boldsymbol{b}$. Hence, we devised a strategy to make experiment-specific predictions.

Our optogenetic experiments include both regional and axonal inactivation experiments. An important technical consideration is that the extent of inhibition of an area's output achieved by regional or axonal optogenetics may not be equivalent. Likewise, behavioral deficits caused by these manipulations may not be equivalent. We resolved this issue by scaling the observed changes in behavioral performance b_j in each experiment by a positive coefficient that accounts for the reliability of the inactivation method used (w_j). An important consequence of expressing behavioral performance in this way is that it allows us to decompose $\boldsymbol{b}$ into its components. We defined the

behavioral performance vector $\boldsymbol{b}$ by a control performance vector $b_{control}$ (all entries in $b_{control}$ are 1, denoting baseline behavioral performance) from which the change in error rate observed on each optogenetic experiment is subtracted. Specifically, $\boldsymbol{b} = w_{control}b_{control} - w_{ACC-SC}b_{ACC-SC} - w_{ACC}b_{ACC} - w_{SC}b_{SC}$, where each w_j is a fixed non-negative scalar and $b_{ACC\text{-}SC}$, b_{ACC}, and b_{SC} are the following vectors:

$$b_{ACC\text{-}SC} = \begin{bmatrix} 0 \\ 0 \\ err^{c}_{ACC-SC} \\ err^{i}_{ACC-SC} \\ 0 \\ 0 \\ 0 \\ 0 \end{bmatrix} \quad b_{ACC} = \begin{bmatrix} 0 \\ 0 \\ 0 \\ 0 \\ err^{c}_{ACC} \\ err^{i}_{ACC} \\ 0 \\ 0 \end{bmatrix} \quad b_{SC} = \begin{bmatrix} 0 \\ 0 \\ 0 \\ 0 \\ 0 \\ 0 \\ err^{c}_{SC} \\ err^{i}_{SC} \end{bmatrix}$$

The term err in these vectors is the laser-induced change in the error rate (i.e., error $\text{rate}_{\text{laser}}$ – error $\text{rate}_{\text{nonlaser}}$), with subscript and superscript denoting the experiment and the trial-type, respectively.

We derived experiment-dependent estimates by defining the following system of equations for each of the three experiments: $Ax_{ACC-SC} = b_{ACC-SC}$, $Ax_{ACC} = b_{ACC}$, and $Ax_{SC} = b_{SC}$, where each x_j is the contribution of the four input pathways to activity in the SC as derived from the corresponding optogenetic experiment. Each linear system defined by $Ax_j = b_j$ has more equations than variables and, generally, does not have a unique solution. Hence, we derived estimates $\hat{x}_j$ that best approximate the relationship $A\hat{x}_j = b_j$ by minimizing the squared Euclidean distance $\| A\hat{x}_j - b_j \|^2$. The optimal $\hat{x}_j$ estimated from each optogenetic experiment is given by least-squares approximation[64], defined generically as $\hat{x}_j = (A^TA)^{-1}A^Tb_j$. Note that all rows except the two corresponding to the specific experiment considered in each experiment-specific b_j are set to 0 (i.e., no change in behavioral performance). Hence, each estimate $\hat{x}_j$ is interpreted as the change in activity along the four inputs to SC_m that is required to best approximate the change in behavioral performance caused by the corresponding inactivation experiment, relative to the activity that would cause no change in behavioral performance. For instance, the estimate $\hat{x}_{SC}$ shows that the decrease in contraversive bias observed by inactivating the SC in the model is best explained if the D pathway normally contributes significant

excitation to the SC. Inhibiting this input through optogenetic inactivation of the left SC reduces activity in SC_L, hence causing the observed decrease in contraversive bias.

We used each estimated $\hat{x}_j$ to predict the effect of inactivating the ACC-VC pathway on behavior. We simulated the inactivation of the left ACC-VC projection in the model by nulling the contribution of $E_{ACC\text{-}VC\text{-}SC}$ in eq 1. shown in Extended Data Fig. 11A, defining the following matrix:

$$\begin{bmatrix} c & -(1-c) & 0 & 1 \\ 1-c & -c & 1-c & 1 \end{bmatrix}$$

From this matrix, we derived a 2-by-4 matrix *P* whose first and second row correspond to $SC_L(\mathrm{c}) - SC_R(\mathrm{c})$ and $SC_R(i) - SC_L(i)$, as done for making the matrix *A* (Extended Data Fig 11D). Using the $\hat{x}_j = (A^TA)^{-1}A^Tb_j$ relationship defined above, we reasoned that the predicted change in behavioral performance during ACC-VC inactivation, $b_{j\text{-}pred}$, for each estimated $\hat{x}_j$ is given by $P\hat{x}_j = b_{j\text{-}pred.}$ Hence, by substituting for $\hat{x}_j$, we defined $b_{j\text{-}pred} = P\,(A^TA)^{-1}\,A^T\,b_j$. The variables c *and* i in A represent the drive provided by the ACC on contraversive and ipsiversive trials, respectively. We set these variables based on the observed proportion of ACC-SC neurons preferentially active on contraversive and ipsiversive trials, respectively ($c = 0.65$ and $i = 0.35$; Fig. 3D) and calculated $b_{j\text{-}pred}$ for all three experiments. We found that each of the three experiments predicted that inactivating the $E_{ACC\text{-}VC\text{-}SC}$ pathway in the model leads to a decrease in contraversive orienting. Thus, by aggregating the experimental data regardless of their reliability, our analysis predicts that experimentally inactivating the ACC-VC pathway should decrease contraversive orienting.

Methods references

51. Wickersham, I. R. & Sullivan, H. A. Rabies viral vectors for monosynaptic tracing and targeted transgene expression in neurons. *Cold Spring Harb. Protoc.* **2015,** 375–385 (2015).
52. Wickersham, I. R., Sullivan, H. A. & Seung, H. S. Production of glycoprotein-deleted rabies viruses for monosynaptic tracing and high-level gene expression in neurons. *Nat. Protoc.* **5,** 595–606 (2010).
53. Raymond, C. S. & Soriano, P. High-efficiency FLP and ΦC31 site-specific recombination in mammalian cells. *PLoS One* **2,** e162 (2007).
54. Choi, V. W., Asokan, A., Haberman, R. A., McCown, T. J. & Samulski, R. J.

Production of recombinant adeno-associated viral vectors and use for in vitro and in vivo administration. *Curr. Protoc. Neurosci.* **Chapter 4,** Unit 4.17 (2006).

55. Franklin, K. B. J. & Paxinos, G. *Paxinos and Franklin's The mouse brain in stereotaxic coordinates*. (Elsevier/Academic Press, Boston, MA, 2013).
56. Madisen, L. *et al.* Transgenic mice for intersectional targeting of neural sensors and effectors with high specificity and performance. *Neuron* **85,** 942–58 (2015).
57. Tallquist, M. D. & Soriano, P. Epiblast-restricted Cre expression in MORE mice: a tool to distinguish embryonic vs. extra-embryonic gene function. *Genesis* **26,** 113–5 (2000).
58. Tseng, Q. *et al.* A new micropatterning method of soft substrates reveals that different tumorigenic signals can promote or reduce cell contraction levels. *Lab Chip* **11,** 2231 (2011).
59. Chen, T.-W. *et al.* Ultrasensitive fluorescent proteins for imaging neuronal activity. *Nature* **499,** 295–300 (2013).
60. Chang, C.-C. & Lin, C.-J. LIBSVM: A library for support vector machines. *ACM Trans. Intell. Syst. Technol.* **2,** 1–27 (2011).
61. Panzeri, S., Harvey, C. D., Piasini, E., Latham, P. E. & Fellin, T. Cracking the Neural Code for Sensory Perception by Combining Statistics, Intervention, and Behavior. *Neuron* **93,** 491–507 (2017).
62. Armstrong, K. M., Chang, M. H. & Moore, T. Selection and Maintenance of Spatial Information by Frontal Eye Field Neurons. *J. Neurosci.* **29,** 15621–15629 (2009).
63. Chung, J. E. *et al.* A Fully Automated Approach to Spike Sorting. *Neuron* **95,** 1381–1394.e6 (2017).
64. Strang, G. *Introduction to linear algebra*. **5.** (Wellesley-Cambridge Press, Wellesley, MA, 2016).